Neurobiology of Disease 79 (2015) 150–163

Contents lists available at ScienceDirect

Neurobiology of Disease

journal homepage: www.elsevier.com/locate/ynbdi

Effects of impaired membrane interactions on α-synuclein aggregation and neurotoxicity

Daniel Ysselstein [a], Mehul Joshi [a], Vartika Mishra [a], Amy M. Griggs [a,1], Josephat M. Asiago [a], George P. McCabe [b], Lia A. Stanciu [c], Carol Beth Post [a], Jean-Christophe Rochet [a,*]

[a] Department of Medicinal Chemistry and Molecular Pharmacology, Purdue University, West Lafayette, IN, USA
[b] Department of Statistics, Purdue University, West Lafayette, IN, USA
[c] Schools of Materials Engineering and Biomedical Engineering, Purdue University, West Lafayette, IN, USA

ARTICLE INFO

Article history:
Received 21 January 2015
Revised 20 April 2015
Accepted 21 April 2015
Available online 27 April 2015

Keywords:
Aggregation
α-Helix
α-Synuclein
Familial mutation
Membrane
Neurodegeneration
Oligomer
Parkinson's disease
Phospholipid
Vesicle

ABSTRACT

The post-mortem brains of individuals with Parkinson's disease (PD) and other synucleinopathy disorders are characterized by the presence of aggregated forms of the presynaptic protein α-synuclein (aSyn). Understanding the molecular mechanism of aSyn aggregation is essential for the development of neuroprotective strategies to treat these diseases. In this study, we examined how interactions between aSyn and phospholipid vesicles influence the protein's aggregation and toxicity to dopaminergic neurons. Two-dimensional NMR data revealed that two familial aSyn mutants, A30P and G51D, populated an exposed, membrane-bound conformer in which the central hydrophobic region was dissociated from the bilayer to a greater extent than in the case of wild-type aSyn. A30P and G51D had a greater propensity to undergo membrane-induced aggregation and elicited greater toxicity to primary dopaminergic neurons compared to the wild-type protein. In contrast, the non-familial aSyn mutant A29E exhibited a weak propensity to aggregate in the presence of phospholipid vesicles or to elicit neurotoxicity, despite adopting a relatively exposed membrane-bound conformation. Our findings suggest that the aggregation of exposed, membrane-bound aSyn conformers plays a key role in the protein's neurotoxicity in PD and other synucleinopathy disorders.

Introduction

Parkinson's disease (PD) is an age-related neurodegenerative disorder defined by the presence of cytoplasmic inclusions named Lewy bodies, which contain aggregated forms of the protein α-synuclein (aSyn) (Rochet et al., 2012; Shulman et al., 2011; Spillantini et al., 1997). aSyn is a highly expressed protein that localizes to presynaptic nerve terminals. Several autosomal dominant mutations in the SNCA gene encoding aSyn have been linked to familial forms of PD, including substitutions (A30P, E46K, H50Q, G51D, A53E, and A53T) (Kiely et al., 2013; Kruger et al., 1998; Lesage et al., 2013; Pasanen et al., 2014; Polymeropoulos et al., 1997; Proukakis et al., 2013; Shulman et al., 2011; Zarranz et al., 2004) and gene multiplications (Chartier-Harlin et al., 2004; Singleton et al., 2003). Some of the substitution mutants have been shown to have an increased propensity to form high molecular weight oligomers (Conway et al., 2000; Greenbaum et al., 2005; Li et al., 2001), and gene multiplications are predicted to promote aSyn aggregation via mass action (Rochet et al., 2012). These observations suggest that aSyn oligomerization is a key event in PD pathogenesis. Additionally, aSyn accumulation has been observed in other neurodegenerative diseases referred to as 'synucleinopathies', including dementia with Lewy bodies and multiple system atrophy (Spillantini et al., 1997; Wakabayashi et al., 1998). A better understanding of the events that initiate aSyn aggregation is critical for designing neuroprotective strategies to treat PD and other synucleinopathy disorders.

aSyn is most commonly expressed as a 14 kDa (140-residue) protein. Biophysical studies have revealed that the protein is natively unfolded in solution (Weinreb et al., 1996). The protein consists of 3 regions: an N-terminal region, a central hydrophobic region, and a C-terminal region (Fig. 1A). The N-terminal region spans the first 67 amino acid residues and contains 5 conserved lysine-rich repeats. The

Abbreviations: aSyn, α-synuclein; CD, circular dichroism; DOPC, 1,2-dioleoyl-*sn*-glycero-3-phosphocholine; DOPE, 1,2-dioleoyl-*sn*-glycero-3-phosphoethanolamine; DOPS, 1,2-dioleoyl-*sn*-glycero-3-phospho-L-serine; EGFP, enhanced green fluorescent protein; HSQC, heteronuclear single quantum coherence; MAP2, microtubule associated protein 2; MOI, multiplicity of infection; PBS-T, PBS + Tween 20; PC, L-α-phosphatidylcholine; PD, Parkinson's disease; PG, L-α-phosphatidylglycerol; POPG, 1-palmitoyl-2-oleoyl-*sn*-glycero-3-phosphoglycerol; PUFA, polyunsaturated fatty acid; SUV, small unilamellar vesicle; TH, tyrosine hydroxylase.

* Corresponding author at: Department of Medicinal Chemistry and Molecular Pharmacology, Purdue University, 575 Stadium Mall Drive, West Lafayette, IN, USA. Fax: +1 765 494 1414.
E-mail address: jrochet@purdue.edu (J.-C. Rochet).
[1] Present address: Cook Research Incorporated, West Lafayette, IN, USA.
Available online on ScienceDirect (www.sciencedirect.com).

http://dx.doi.org/10.1016/j.nbd.2015.04.007
0969-9961/

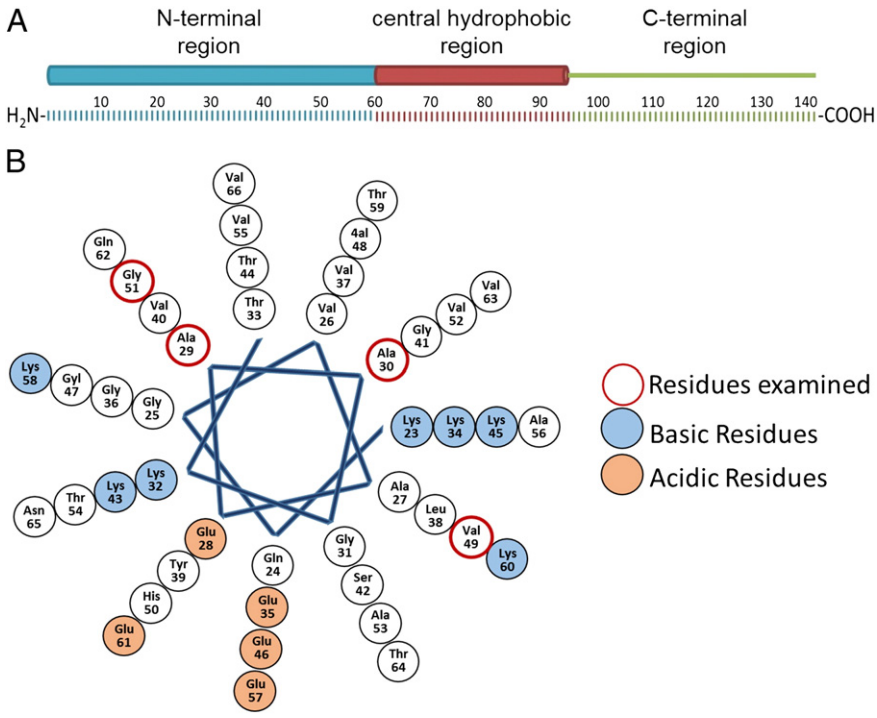

Fig. 1. aSyn adopts an α-helical structure upon binding phospholipid membranes. (A) Schematic representation of the secondary structure of membrane-bound aSyn. The amphipathic α-helix, shown here spanning the N-terminal region (blue) and the central hydrophobic region (red), and the unfolded C-terminal region (green) are depicted above a map of the polypeptide chain with identical color coding. (B) Helical wheel plot portraying residues 23–66 in the membrane-binding region of aSyn as an amphipathic α11/3 helix. Because A29 and G51 are located on the hydrophobic face of the helix embedded in the membrane, replacement of either residue by an acidic residue is predicted to disfavor membrane binding and helix formation. In contrast, V49 is located on the hydrophilic face of the helix exposed to solvent. Accordingly, the replacement of this residue with an acidic residue should have a less pronounced effect on membrane binding and helix formation, though the proximity of residue 49 to the predicted membrane interface suggests that a negative charge at this position could be repelled by anionic lipid head groups. Residues examined in this study are outlined in red. Basic and acidic residues are highlighted with blue and orange shading, respectively.

central region (spanning residues 61–95) is highly hydrophobic and contains a 6th lysine-rich repeat. Within the central region, residues 71–82 are required for aggregation of the protein (Giasson et al., 2001). The C-terminal region spanning residues 96–140 contains many proline residues and acidic residues and is thought to be involved in long-range interactions that stabilize the protein and prevent aggregation (Bertoncini et al., 2005; Dedmon et al., 2005).

The ability of aSyn to bind phospholipid membranes has been well documented and is presumably necessary for the protein's function in regulating synaptic vesicle trafficking (Davidson et al., 1998; Jensen et al., 1998; Venda et al., 2010). A number of groups have shown that aSyn interacts with anionic phospholipid vesicles or detergent micelles by forming an amphipathic α-helix (most likely an α11/3 helix) with various lengths, ranging from a short helix spanning residues ~1–25 to a long helix spanning residues ~1–97 and including the central hydrophobic region (Bartels et al., 2010; Bodner et al., 2009, 2010; Bussell and Eliezer, 2003; Davidson et al., 1998; Jao et al., 2004; Jo et al., 2000) (Fig. 1A). The protein adopts a predominantly broken or continuous α-helical structure upon binding high- or low-curvature membranes, respectively (Chandra et al., 2003; Ferreon et al., 2009; Georgieva et al., 2010; Trexler and Rhoades, 2009; Ulmer et al., 2005). Interactions involving an N-terminal segment spanning residues 1–25 are critical for membrane binding and for the adoption of an α-helical structure (Bartels et al., 2010).

aSyn has been shown to undergo accelerated aggregation at the membrane surface when incubated with isolated rat membrane homogenates (Lee et al., 2002), synaptosomal membranes (Jo et al., 2004), exosomes (Grey et al., 2015), detergent micelles (Giehm et al., 2010; Necula et al., 2003), phospholipid vesicles (Galvagnion et al., 2015), and supported phospholipid bilayers (Haque et al., 2010; Pandey et al., 2009) at relatively high protein:lipid ratios. The increased propensity of aSyn to undergo aggregation in the presence of membranes versus in solution could be because the two dimensional surface of the lipid bilayer increases the probability of molecular interactions needed for oligomerization (Abedini and Raleigh, 2009; Pandey et al., 2009). It has also been observed that aSyn exhibits an enhanced propensity to form high molecular weight aggregates in the presence of polyunsaturated fatty acids (PUFAs) (Perrin et al., 2001; Sharon et al., 2003). PUFAs are thought to stimulate aSyn self-assembly because they are susceptible to oxidation to 4-hydroxy-2-nonenal and 4-oxo-2-nonenal, and the incubation of aSyn with these oxidation products results in the formation of large, covalently crosslinked β-sheet-rich oligomers (Nasstrom et al., 2011; Qin et al., 2007). Membrane-induced aSyn aggregation may play a role in neurodegeneration by triggering membrane thinning, a process that could result in increased ion permeability (Comellas et al., 2012; Lee et al., 2012; Ouberai et al., 2013; Pfefferkorn et al., 2012; Reynolds et al., 2011).

Although evidence suggests that phospholipid membranes can stimulate aSyn aggregation, conformational properties of membrane-bound aSyn favoring its self-assembly are poorly understood. We hypothesize that structural perturbations which disrupt interactions between the central hydrophobic region and the phospholipid bilayer promote the formation of neurotoxic aSyn aggregates at the membrane surface. To address this hypothesis, we characterized a set of aSyn mutants (A29E, A30P, V49E, G51D) in terms of their membrane affinity, membrane-bound conformation, propensity to undergo membrane-induced aggregation, and neurotoxicity as compared to WT aSyn. The rationale for examining these mutants was that their amino acid substitutions were predicted to disrupt aSyn-phospholipid interactions at various sites on the amphipathic α11/3 helix formed by the membrane-bound protein (Fig. 1B). Our findings suggest a molecular basis for the enhanced neurotoxicity of the familial mutants A30P and G51D, and they yield insight into the molecular features of aSyn that

modulate membrane binding, membrane-induced aggregation, and neurotoxicity.

Materials and methods

Materials

Unless otherwise stated all chemicals were purchased from Sigma Chemical Co. (St. Louis, MO). ^{15}N-labeled NH_4Cl was obtained from Cambridge Isotope Laboratories (Tewksbury, MA). L-α-Phosphatidylcholine (PC), L-α-phosphatidylglycerol (PG), and a mixture of 1,2-dioleoyl-*sn*-glycero-3-phosphoethanolamine (DOPE):1,2-dioleoyl-*sn*-glycero-3-phospho-L-serine (DOPS):1,2-dioleoyl-*sn*-glycero-3-phosphocholine (DOPC) (5:3:2 w/w/w) were purchased from Avanti Polar Lipids (Alabaster, AL). Iodixanol, phospholipid extrusion membranes, and ECF substrate were obtained from GE Healthcare Life Sciences (Pittsburgh, PA). 100 kDa spin filters were purchased from Millipore (Billerica, MA). DMEM, penicillin–streptomycin, the ViraPower Adenoviral Expression System, and LR clonase were obtained from Invitrogen (Carlsbad, CA). The Adeno-X qPCR titration kit was purchased from Clontech (Mountain View, CA). FBS was obtained from Sigma Chemical Co. or Atlanta Biologicals (Flowery Branch, GA). Nuserum and BCA assay reagents were purchased from Thermo Fisher Scientific (Waltham, MA).

Antibodies

The following antibodies were used in these studies: mouse anti-aSyn (Syn-1, catalog number 610787, BD Biosciences, San Jose, CA); AP-linked anti-mouse (Cell Signaling Technology, Danvers, MA); chicken anti-MAP2 (catalog number CPCA-MAP2, EnCor Biotechnology, Gainesville, FL); rabbit anti-TH (catalog number AB152, Millipore, Billerica, MA); and anti-rabbit IgG-Alexa Fluor 488, anti-rabbit IgG-Alexa Fluor 594, and anti-chicken IgG-Alexa Fluor 594 (Invitrogen, Carlsbad, CA).

Protein preparation

The pT7-7 constructs encoding A29E and V49E were a gift from Dr. Peter Lansbury and Dr. Michael Volles (Harvard Medical School) (Volles and Lansbury, 2007). A cDNA encoding G51D was generated via overlap-extension PCR and subcloned as an NdeI–BamHI fragment into the pT7-7 expression vector. Recombinant aSyn was purified from BL21 (DE3) cells transformed with pT7-7 constructs encoding WT or mutant aSyn as described (Zhang et al., 2013). To generate ^{15}N-labeled proteins for NMR analysis, *E. coli* cells transformed with pT7-7 constructs were grown overnight in LB media and then diluted into minimal media containing ^{15}N-NH_4Cl for protein expression as described (Marley et al., 2001). Prior to each experiment, protein solutions prepared by resuspending purified, lyophilized aSyn variants were filtered by successive centrifugation steps through a 0.22 μm spin filter and a 100 kDa centrifugal filter to remove aggregates and oligomers.

Lipid vesicle preparation

Egg PG and egg PC suspended in chloroform were mixed at equimolar ratios in a round bottom flask. The PG:PC lipid mixture or a mixture of DOPE:DOPS:DOPC (5:3:2 w/w/w) was dried under a nitrogen stream and placed in a vacuum drier for 2 h to ensure complete removal of the chloroform. The dried lipids were suspended in PBS (10 mM phosphate buffer, 2.7 mM KCl, and 137 mM NaCl, pH 7.4), and small unilamellar vesicles (SUVs) were prepared by extruding the suspension through a 50 nm Whatman membrane 20 times using a mini-extruder system. The diameter of the SUVs was found to be between 50 and 70 nm by dynamic light scattering on a Zetasizer Nano ZS instrument (Malvern Instruments, Worcestershire, UK). SUVs were stored at 4 °C prior to use.

Circular dichroism

Far-UV circular dichroism (CD) measurements were performed using a Chirascan SC spectrometer (Applied Photophysics, Leatherhead, UK). Solutions of recombinant aSyn (5 μM in 20 mM KP_i, pH 7.4) in the absence or presence of SUVs (lipid:protein ratio, 50:1 to 1600:1 mol/mol) were analyzed in a 1 mm quartz cuvette at 22 °C. The ellipticity at 222 nm was recorded, and the data were background corrected (eliminating signals associated with the buffer and SUVs) by subtracting ellipticity values obtained for equivalent samples minus protein. The mean residue molar ellipticity at 222 nm ($[\theta]_{MR,\,222}$) was calculated using the following equation:

$$[\theta]_{MR,\,222} = \theta_{222}/10\mathrm{Cnl} \tag{1}$$

where θ_{222} is the observed (background corrected) ellipticity at 222 nm in millidegrees, C is the protein concentration in M, n is the number of amino acid residues in the protein (= 140), and l is the path length of the cuvette in cm. Binding curves generated by plotting $[\theta]_{MR,\,222}$ versus the lipid concentration were analyzed by fitting to the following equation:

$$R = R_0 - (R_0 - R_f)\frac{K_d + C + L/N - \sqrt{(K_d + C + L/N)^2 - 4CL/N}}{2C} \tag{2}$$

where R is the measured $[\theta]_{MR,\,222}$ at a given lipid concentration, R_0 is the $[\theta]_{MR,\,222}$ in the absence of lipid, R_f is the $[\theta]_{MR,\,222}$ in the presence of saturating lipid, L is the total lipid concentration, C is the total protein concentration, K_d is the apparent macroscopic dissociation equilibrium constant, and N is the binding stoichiometry (lipids/protein) (Shvadchak et al., 2011a). The data obtained for WT aSyn were fit to Eq. (2) via non-linear regression with R_0, R_f, K_d, and N as unconstrained parameters. The data obtained for the aSyn mutants were fit to Eq. (2) with N set to a value determined from the fit of the WT aSyn data (N = 280 or 300 for WT aSyn incubated with PG:PC vesicles or PE:PS:PC vesicles, respectively). This approach of constraining N, necessary to obtain a satisfactory fit of the binding data for the lower-affinity aSyn mutants, is reasonable based on the assumption that the stoichiometry of binding to SUVs with a particular phospholipid composition should be approximately equal for WT aSyn and variants with the same number of residues (Shvadchak et al., 2011a).

To determine the maximum helical content of each aSyn variant, we used the following equations:

$$H = 100\% \cdot \frac{(\theta - \theta_{coil})}{(\theta_\alpha - \theta_{coil})} \tag{3}$$

$$\theta_\alpha = -40000(1 - 2.5/n) + 100t \tag{4}$$

$$\theta_{coil} = 640 - 45t \tag{5}$$

where H is the maximum % helicity, θ is the $[\theta]_{MR,\,222}$ in the presence of saturating lipid (R_f in Eq. 2), θ_α is the $[\theta]_{MR,\,222}$ value of an idealized α-helical peptide, θ_{coil} is the $[\theta]_{MR,\,222}$ value of an idealized random coil peptide, n is the number of amino acid residues in the protein (= 140), and t is the temperature (22 °C) (Scholtz et al., 1991; Shvadchak et al., 2011b).

2D NMR analysis

NMR measurements were carried out using a Bruker Advance 800 MHz spectrometer equipped with a room temperature probe (Billerica, MA). Solutions of ^{15}N-labeled aSyn (150 μM in 20 mM KP_i, pH 7.4, 90% H_2O/10% D_2O (v/v)) in the absence or presence of SUVs

(lipid:protein ratio, 20:1 mol/mol) were analyzed at 10 °C. 2D NMR analyses were carried out by recording ^{1}H–^{15}N heteronuclear single quantum coherence (HSQC) spectra with a data matrix of 2048 (F2, ^{1}H) × 256 (F1, ^{15}N) increments in the direct and indirect dimensions, respectively. The spectra were processed with NMRPipe (Delaglio et al., 1995). Assignments listed in the BioMagResBank database (accession number, 18857) matched assignments shown in a previous report (Eliezer et al., 2001) and were used in this study. Only small chemical shift changes were observed for ≤3 residues immediately bracketing the substitution site, consistent with previous findings (Bodner et al., 2010). Peak intensities (heights) were determined using Sparky (T.D. Goddard and D.G. Kneller, University of California San Francisco). To monitor residue-specific interactions of aSyn with the membrane, the fractional signal attenuation of each residue peak in the presence versus the absence of SUVs was determined as described (Bodner et al., 2009; Bodner et al., 2010).

Lipid flotation assay

Solutions of recombinant aSyn in PBS with 0.02% (w/v) NaN_3 were incubated with PG:PC SUVs (lipid:protein ratio, 20:1 mol/mol) at 37 °C for 72 or 96 h in a total volume of 60 μL. The final concentration of aSyn in the protein–lipid mixture was 100 μM (determined with a BCA Protein Assay Kit). After incubation, each sample was mixed with 4 mL of 30% (v/v) iodixanol solution and overlaid with 7.0 mL of 25% (v/v) iodixanol and 350 μL of 5% (v/v) iodixanol in a polyalomar tube (Beckman, Miami, FL). All of the above iodixanol solutions were prepared in lipid flotation buffer (10 mM HEPES, pH 7.4, 150 mM NaCl). The samples were spun at 200,000 ×*g* in a Beckman SW 41 Ti rotor for 4 h at 4 °C. The membrane fraction was carefully collected from the 5% iodixanol layer at the top of the gradient and diluted in 11 mL of lipid flotation buffer. Membrane-bound proteins were pelleted via centrifugation at 200,000 ×*g* for 2 h at 4 °C, resuspended in 250 μL of PBS, and stored at −20 °C prior to Western blot analysis. In general we found that the rate of aSyn aggregation increased in the presence of SUVs that had been stored for ~3–4 weeks at 4 °C, apparently because oxidized phospholipids that accumulated during vesicle storage promoted aSyn–membrane binding and self-assembly of the protein at the membrane surface (Griggs, A.M. and Rochet, J.-C., unpublished data).

Western blot analysis

Membrane-bound aSyn isolated by lipid flotation was analyzed by Western blotting. Protein samples were combined with Laemmli buffer (final concentration, 60 mM Tris–HCl, pH 6.8, 2% (w/v) SDS, 10% (v/v) glycerol, 5% (v/v) β-mercaptoethanol, 0.01% (w/v) bromophenol blue) and boiled for 5 min. Denatured proteins were separated via SDS-PAGE on a 4–20% (w/v) polyacrylamide gradient gel (BioRad, Hercules, CA) and transferred to a PVDF membrane (pore size, 0.4 μm). After blocking in 10% (w/v) non-fat milk, the membrane was washed with PBS + 0.5% (w/v) Tween 20 (PBS-T) and probed for aSyn with the Syn-1 primary antibody, diluted 1/1500 in PBS-T with 1% (w/v) BSA. After washing in PBS-T, the membrane was probed with a secondary anti-mouse antibody conjugated to alkaline phosphatase (diluted 1/5000). To visualize the bands, the membrane was exposed to ECF substrate for 30 s, and images were acquired using a Typhoon imaging system (GE Life Sciences, Pittsburgh, PA). Band densities were quantified using ImageJ software (NIH, Bethesda, MD).

Preparation of adenoviral constructs

Adenoviruses expressing aSyn variants were prepared using the ViraPower Adenoviral Expression System (Liu et al., 2008). cDNAs encoding WT or mutant aSyn were subcloned as KpnI–XhoI fragments into the entry vector pENTR1A, and the inserts from the pENTR1A constructs were then transferred into the pAd/CMV/V5 adenoviral expression vector via recombination using Gateway LR Clonase.

A cDNA encoding enhanced green fluorescent protein (EGFP) was subcloned as a KpnI–XhoI fragment into pENTR1A, yielding the construct pENTR–EGFP. A DNA fragment encoding the herpes simplex virus thymidine kinase polyadenylation signal (TKpolyA) was amplified from pAd/CMV/V5 by PCR and subcloned as an XhoI–EcoRV fragment into pENTR–EGFP, yielding the construct pENTR–EGFP–TKpolyA. A DNA fragment encoding the human synapsin promoter sequence was excised from the vector pAAV2 by digestion with SmaI and KpnI and subcloned into the vector pENTR–EGFP–TKpolyA cut with XmnI and KpnI, yielding the construct pENTR–synapsin–EGFP–TKpolyA. The synapsin–EGFP–TKpolyA insert from this construct was transferred into the pAd/PL-DEST adenoviral vector via recombination using Gateway LR Clonase. pAd/PL-DEST is a 'promoter-less' version of pAd/CMV/V5 (both have the same sequences required for packaging and production of human adenovirus type 5).

The sequence of the DNA insert in each adenoviral construct was verified using an Applied Biosystems (ABI3700) DNA sequencer (Purdue University). Adenoviral constructs were packaged into virus via lipid-mediated transient transfection of the HEK 293A packaging cell line. Adenovirus packaged with the plasmid pAd/V5-DEST/LacZ (Invitrogen), encoding the control protein β-galactosidase fused to the V5 epitope, was also prepared to control for non-specific effects of viral transduction. Adenoviral titers were determined using the Adeno-X qPCR titration kit.

Analysis of relative aSyn expression levels

Relative expression levels of the aSyn variants encoded by different adenoviral constructs were determined via Western blot analysis. Human SH-SY5Y neuroblastoma cells were plated on 6-well plates at a density of 300,000 cells per well in media consisting of RPMI, 10% (v/v) Nuserum, penicillin (100 U/mL), and streptomycin (100 μg/mL). Two days after plating, the cells were transduced with aSyn adenovirus at a multiplicity of infection (MOI) of 37.5–75. After 72 h, the cells were dislodged from the plate by trypsinization, collected by centrifugation, washed with PBS, and lysed in RIPA buffer (50 mM Tris HCl, pH 7.4, 150 mM NaCl, 0.1% (w/v) SDS, 0.5% (w/v) sodium deoxycholate, 1% (v/v) Triton X-100) with protease inhibitor cocktail (Sigma P8340) and 1 mM PMSF. After centrifugation at 13,000 ×*g*, the detergent-soluble (supernatant) fraction was recovered and assayed for protein concentration using a BCA Protein Assay Kit. Equal amounts of protein were separated via SDS-PAGE on a 12% (w/v) polyacrylamide gel and analyzed via Western blotting as described above for the analysis of membrane-bound aSyn isolated by lipid flotation.

Preparation and treatment of primary mesencephalic cultures

Primary midbrain cultures were prepared via dissection of day 17 embryos obtained from pregnant Sprague–Dawley rats (Harlan, Indianapolis, IN) using the methods approved by the Purdue Animal Care and Use Committee, as described (Cooper et al., 2006; Liu et al., 2008; Strathearn et al., 2014). The mesencephalic region containing the *substantia nigra* and ventral tegmental area was isolated stereoscopically, and the tissue was treated with trypsin (final concentration, 26 μg/mL in 0.9% [w/v] NaCl). Dissociated cells were plated on 48-well plates (pretreated with poly-L-lysine, 5 μg/mL) at a density of 163,500 cells per well in media consisting of DMEM, 10% (v/v) FBS, 10% (v/v) horse serum, penicillin (100 U/mL), and streptomycin (100 μg/mL). Five days after plating, the cells were treated for 48 h with cytosine arabinofuranoside (20 μM, 48 h) to inhibit the growth of glial cells. At this stage (7 days in vitro), the cultures were transduced with adenovirus encoding aSyn, β-galactosidase, or synapsin/EGFP for 72 h at an MOI of 7.5 to 15. The MOIs of adenoviruses encoding aSyn variants were adjusted to ensure equal expression levels based on data from

Western blot analysis of lysates from transduced SH-SY5Y cells as outlined above (for each virus, the MOI used to transduce primary midbrain cultures was 5-fold less than that used for the transduction of SH-SY5Y cells).

After incubation in fresh media for an additional 24 h, the cells were fixed in 4% (w/v) paraformaldehyde in PBS and subsequently permeabilized for 1 h with PBS, 0.3% (v/v) Triton X-100, 1% (w/v) BSA, and 10% (v/v) FBS. For experiments aimed at monitoring relative dopaminergic cell viability or neurite lengths, the cells were treated for 48 h at 4 °C with chicken anti-MAP2 (1:2000) and rabbit anti-TH (1:500) primary antibodies. The cells were then washed with PBS and treated with Alexa Fluor 594 goat anti-chicken and Alexa Fluor 488 goat anti-rabbit secondary antibodies (both at 1:1000) for 1 h at 22 °C. For experiments aimed at determining adenoviral transduction efficiencies, cells transduced with virus encoding EGFP downstream of the synapsin promoter were treated for 48 h at 4 °C with chicken anti-MAP2 (1:2000) or rabbit anti-TH (1:500) primary antibody. The cells were then washed with PBS and treated with Alexa Fluor 594 goat anti-chicken or Alexa Fluor 594 goat anti-rabbit secondary antibody (both at 1:1000) for 1 h at 22 °C. After a final wash with PBS, prolong gold antifade reagent with DAPI was applied to each culture well before sealing with a coverslip.

Measurements of primary dopaminergic cell viability

Relative dopaminergic cell viability was assessed by counting MAP2- and TH-immunoreactive primary neurons in a blinded manner using a Nikon TE2000-U inverted fluorescence microscope (Nikon Instruments, Melville, NY) equipped with a 20× objective (Cooper et al., 2006; Liu et al., 2008; Strathearn et al., 2014). A minimum of 10 random fields of view were chosen to provide representation of the whole well. Approximately 300–500 $MAP2^+$ neurons were counted per experiment for each treatment. Each experiment was repeated using cultures isolated from at least 3 different pregnant rats. The data are expressed as the percentage of $MAP2^+$ neurons that were also TH^+ (this ratiometric approach was used to correct for variations in cell plating density).

Neurite length measurements

Neurite length measurements were carried out on the identical primary midbrain cultures used to determine dopamine neuron viability. Images were taken with the automated Cytation 3 Cell Imaging Reader (BioTek, Winooski, VT) using a 4× objective. Lengths of $MAP2^+$ processes extending from $TH^+/MAP2^+$ neurons with an intact cell body (~90 neurons per sample) were assessed in a blinded manner using Nikon NIS Elements analysis software (Nikon Instruments, Melville, NY) (Strathearn et al., 2014).

Statistical analysis

Densitometry data from Western blots and primary neuron viability data were analyzed via ANOVA followed by Tukey's multiple comparisons post hoc test using GraphPad Prism 6.0 (La Jolla, CA). In analyzing percentage cell viability data by ANOVA, square root transformations were carried out to conform to ANOVA assumptions. Neurite length data were analyzed using an approach that accounts for (i) the possibility of multiple neurites arising from a single cell and (ii) the comparison across experiments conducted on different days. Neurite lengths for multiple treatment groups were compared using a general linear model implemented in the GLM procedure of SAS Version 9.3 followed by Tukey's multiple comparisons post hoc test (Cary, NC).

Results

Membrane affinity and membrane-bound conformation of A30P and G51D

The goal of this study was to understand how site-specific perturbations of the amphipathic helical structure of membrane-bound aSyn impact aSyn aggregation at the membrane surface and aSyn neurotoxicity. As a first step, we characterized the familial mutants A30P and G51D in terms of their membrane affinity and membrane-bound conformation, with the aim of then assessing how these properties relate to the variants' relative propensities to undergo membrane-induced aggregation and elicit dopaminergic cell death (see next sections). We focused initially on A30P and G51D because of their importance as familial PD mutants. A30P has been shown by several groups to have a reduced affinity for phospholipids (Jensen et al., 1998; Jo et al., 2002; Perrin et al., 2000), and the G51D substitution was predicted to interfere with aSyn–membrane interactions by placing a negative charge on the non-polar face of the amphipathic α11/3 helix (Fig. 1B).

Recombinant, monomeric WT aSyn, A30P, and G51D were incubated with 50 nm SUVs at lipid:protein ratios of 50:1 to 1600:1 (mol/mol). The SUVs had the following lipid compositions: (i) egg PG:egg PC (1:1 mol/mol) and (ii) DOPE:DOPS:DOPC (5:3:2 w/w/w). These lipid compositions were chosen as each contains anionic lipids necessary for aSyn membrane interactions (Davidson et al., 1998; Jo et al., 2000). In addition, PG:PC vesicles were used in our previous studies (Haque et al., 2010; Pandey et al., 2009; Zakharov et al., 2007), and SUVs consisting of DOPE:DOPS:DOPC have a composition similar to that of synaptic vesicles (Takamori et al., 2006). Changes in aSyn conformation associated with membrane binding were monitored by far-UV CD, a technique that reports on the increase in aSyn α-helicity upon interaction of the protein with phospholipids (Davidson et al., 1998; Jo et al., 2000). Consistent with our previous data (Zakharov et al., 2007), the far-UV CD spectrum of WT aSyn was characterized by (i) a minimum at 198 nm in the absence of SUVs and (ii) a maximum at 192 nm and minima at 208 nm and 222 nm in the presence of SUVs (lipid:protein ratio, 1600:1, mol/mol) (Supplementary Fig. S1).

To compare different aSyn variants in terms of their propensities to adopt an α-helical structure upon binding to SUVs, we used the previously described approach of monitoring the mean residue molar ellipticity at 222 nm ($[\theta]_{MR,\,222}$) as a function of lipid:protein ratio (Scholtz et al., 1991). The data obtained for WT aSyn in the presence of PG:PC vesicles revealed a progressive decrease in $[\theta]_{MR,\,222}$ with increasing lipid:protein ratios (Fig. 2A). The data were fit to Eq. (2) (see 'Materials and methods'), yielding a K_d value of 1.1 ± 0.1 μM, a binding stoichiometry (N value) of 280 lipids per protein, and a maximum α-helical content of 49 ± 1% (Table 1). The lipid titration curves obtained for A30P and G51D in the presence of PG:PC vesicles were shifted to the right compared to the WT aSyn curve, and the K_d values were markedly greater (K_d = 3.2 ± 0.4 μM for A30P and 10 ± 2 μM for G51D) (Fig. 2A, Table 1). Although A30P and WT aSyn exhibited similar α-helical contents in the presence of saturating PG:PC vesicles, the maximum helicity observed for G51D was considerably lower (~43 ± 4%) (Table 1). Analysis of the far-UV CD data obtained for WT aSyn in the presence of DOPE:DOPS:DOPC vesicles yielded a K_d value of 0.21 ± 0.07 μM, a binding stoichiometry of 300 lipids per protein, and a maximum α-helical content of 50 ± 2% (Fig. 2B, Table 1). Here again, A30P and G51D bound to the lipids with higher K_d values (K_d = 2.1 ± 0.5 μM for A30P and 3.1 ± 0.2 μM for G51D), and the maximum helicity observed for G51D (40 ± 2%) was lower than that determined for WT aSyn or A30P. Collectively, these data suggest that (i) G51D and A30P have a reduced affinity for PG:PC and DOPE:DOPS:DOPC vesicles compared to the WT protein; and (ii) the G51D substitution disrupts the α-helical structure of membrane-bound aSyn in the presence of saturating lipid to a greater extent than the A30P substitution.

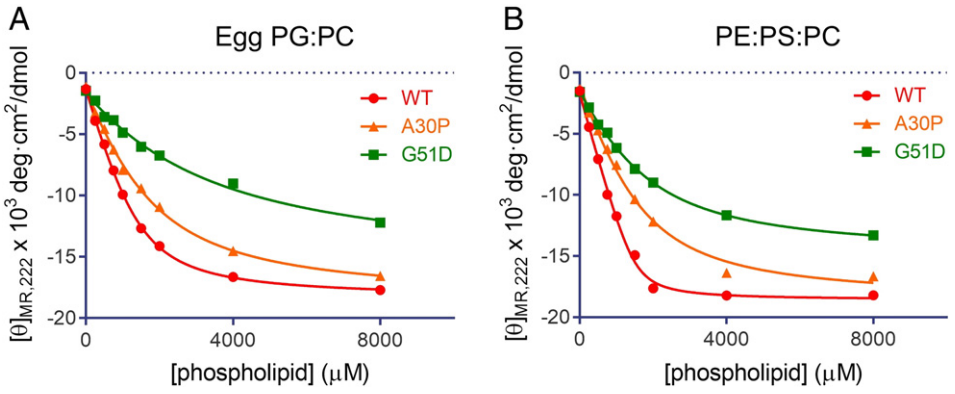

Fig. 2. A30P and G51D display reduced membrane affinity relative to WT aSyn. Solutions of recombinant aSyn variants were analyzed by far-UV CD to determine $[\theta]_{MR,\ 222}$, a measure of protein α-helicity. Each aSyn variant was incubated with increasing concentrations of SUVs composed of egg PG:PC (1:1 mol:mol) (A) or DOPE:DOPS:DOPC (5:3:2 w/w/w) (B). The data were fit to Eq. (2), and values for K_d, minimum $[\theta]_{MR,\ 222}$, and maximum α-helical content were determined from the values of the fit parameters (see Table 1). The data are representative of ≥3 experiments (in total, including both lipid compositions).

To compare the membrane-bound conformations of WT aSyn, A30P, and G51D, ^{15}N-labeled aSyn variants were analyzed via 2D NMR spectroscopy in the absence or presence of DOPE:DOPS:DOPC vesicles, and ^{1}H–^{15}N HSQC spectra were recorded (Figs. 3A and B). This approach is ideal for monitoring residue-specific binding because the signal attenuation of the resonance from a given residue in the presence versus the absence of SUVs is a measure of vesicle binding of that residue. This residue-level monitoring of membrane binding is possible because the partitioning of the residue between a disordered, highly mobile solution state and a membrane-bound state is in the slow-exchange limit on the NMR frequency scale, and the slow rotational motion in the membrane-bound state results in a resonance linewidth too broad for detection. For each residue of aSyn, I/I_0 is the proportion of molecules in an aSyn/SUV mixture in which the residue remains mobile and in solution, and the fractional attenuation $(1 - I/I_0)$ is the proportion of molecules in which the residue is tightly associated with the membrane (Bodner et al., 2009, 2010). Thus, this approach is useful to analyze which residues on the protein are in greatest contact with the lipid vesicle. We used this method to characterize the aSyn–membrane interaction, and in particular to determine whether the central hydrophobic (aggregation-prone) region was either dissociated or associated in the case of conformers referred to here as 'exposed' or 'hidden', respectively. The fractional population of molecules bound to the membrane in either mode ('total bound population') was determined from the mean attenuation of residues 3–9. Our rationale for this approach was that the N-terminal segment of aSyn has a higher membrane affinity compared to more C-terminal regions (Bartels et al., 2010; Drescher et al., 2008; Shvadchak et al., 2011b) and is lipid-bound in the case of both exposed and hidden conformers (Bodner et al., 2010). To calculate the fractional population of protein in the hidden state we determined the mean attenuation of residues 66–80, based on the fact that this segment of the central hydrophobic region contains residues that play a key role in aSyn self-assembly (Giasson et al., 2001), and consistent with a previous report (Bodner et al., 2010). The fractional population of protein with residues 66–80 in the exposed state was determined by subtracting the hidden population from the total bound population. We found that ~84% of WT aSyn molecules were bound to the membrane (Figs. 3C and D; Table 2). Of the total WT protein, ~36% was in the exposed membrane-bound conformation, whereas ~48% was in the hidden state. NMR analysis revealed that ~85% of A30P or G51D molecules were bound to the membrane in the N-terminal region, similar to WT aSyn (Figs. 3C and D; Table 2). However, the percentage of total protein molecules in the exposed state was increased by a factor of 1.9 and 2.0 in the case of A30P and G51D, respectively. For each variant, examination of the sequence dependence of the NMR signal attenuation associated with membrane binding (from N- to C-terminus) revealed that the decrease in attenuation exhibited by A30P or G51D relative to WT aSyn begins in the region of the amino acid substitution, suggesting that the mutation causes a lifting off of the protein from the membrane (Figs. 3E and F).

Table 1
Membrane affinities and maximum helix contents of aSyn variants titrated with SUVs.[a]

PG:PC			
Variant	K_d[b] (μM)	Ellipticity minimum ($\times 10^3$ deg·cm^2/dmol)	Maximum helicity (%)
WT	1.1 ± 0.1	−18 ± 0.2	49 ± 1
G51D	10 ± 2[c]	−16 ± 1	43 ± 4
A30P	3.2 ± 0.4	−18.6 ± 0.4	50 ± 2
A29E	7.5 ± 0.7	−19.7 ± 0.6	53 ± 2
V49E	2.5 ± 0.4	−17.7 ± 0.6	47 ± 2
PE:PS:PC			
Variant	K_d[d] (μM)	Ellipticity minimum ($\times 10^3$ deg·cm^2/dmol)	Maximum helicity (%)
WT	0.21 ± 0.07[e]	−18.6 ± 0.4	50 ± 2
G51D	3.1 ± 0.2[c]	−15.0 ± 0.2	40 ± 2
A30P	2.1 ± 0.5	−18.7 ± 0.8	50 ± 3
A29E	5 ± 1	−21 ± 1	55 ± 4
V49E	1.8 ± 0.4	−18.4 ± 0.8	49 ± 3

[a] Values (± standard error) were determined from the far-UV CD data in Figs. 2 and 6 using Eqs. (2)–(5); the concentration of aSyn was 5 μM.
[b] Fitting of the WT aSyn data to Eq. (2) yielded a binding stoichiometry (*N* value) of 280. The data obtained for the other variants were fit to Eq. (2) with *N* set to a value of 280.
[c] The reduced maximum helicity determined for G51D implies that this variant's *N* value could be lower than that of WT aSyn. Because a fit of the binding data to Eq. (2) with *N* set to a lower value yields an even higher K_d value, the membrane affinity of G51D may in fact be over-estimated.
[d] Fitting of the WT aSyn data to Eq. (2) yielded a binding stoichiometry (*N* value) of 300. The data obtained for the other variants were fit to Eq. (2) with *N* set to a value of 300.
[e] This K_d value is considered approximate because it is 25-fold less than the concentration of protein in the CD experiment.

Membrane-induced self-assembly of A30P and G51D

The CD and NMR data outlined above revealed that introduction of the A30P or G51D mutation led to a significant reduction in lipid interactions involving the central hydrophobic region. As this region plays a key role in aSyn aggregation in solution (Giasson et al., 2001), we postulated that exposure of this region by neighboring aSyn molecules at a high local concentration on the bilayer surface could lead to self-assembly of the protein into membrane-bound aggregates. To address this hypothesis, we incubated each aSyn variant with

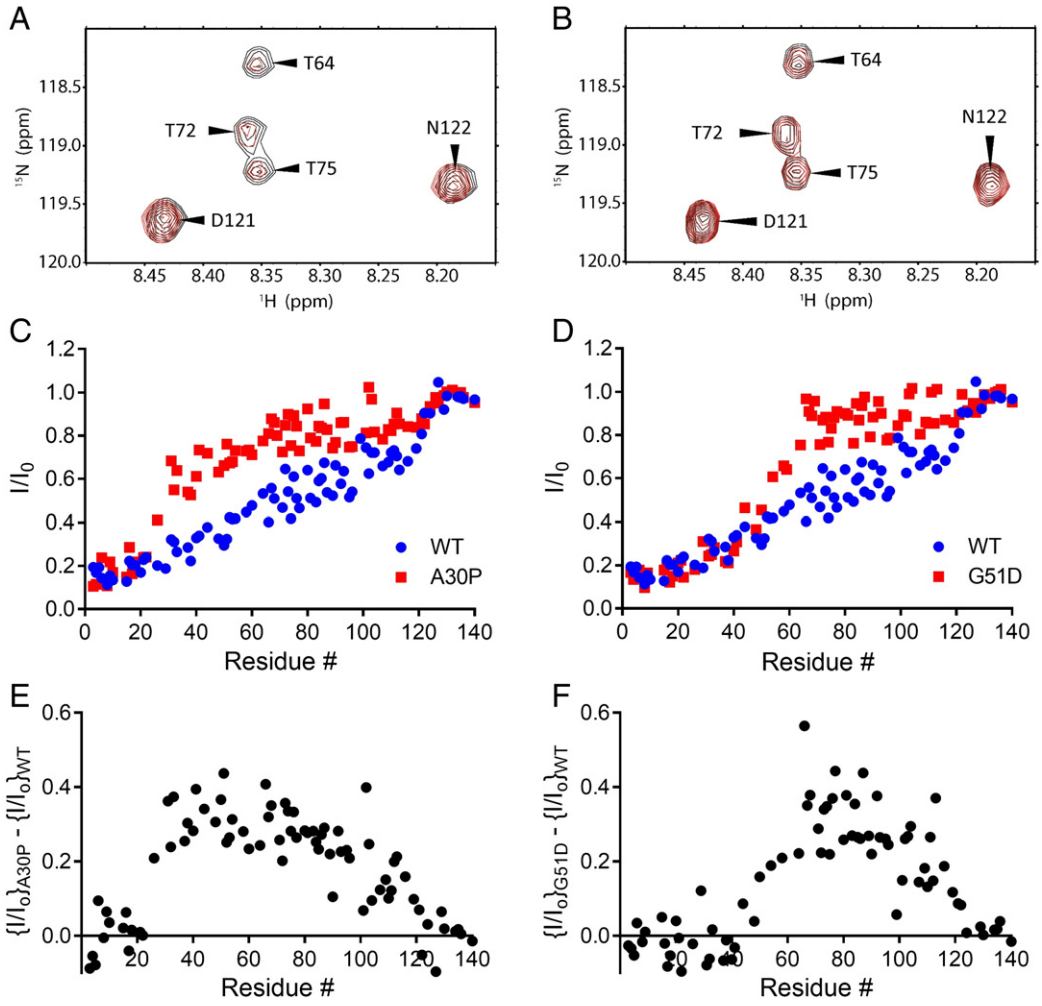

Fig. 3. A30P and G51D have a greater propensity to adopt an exposed membrane-bound conformation than WT aSyn. ^{15}N-labeled aSyn variants were incubated with or without DOPE:DOPS:DOPC SUVs (lipid:protein ratio, 20:1 mol/mol) and analyzed by 2D NMR. (A, B) Selected region of the ^{1}H–^{15}N HSQC spectrum of WT aSyn (A) or G51D (B) in the absence (black) or presence (red) of SUVs. (C, D) Graphs of I/I_0 (where I and I_0 are the peak intensities observed in the presence and absence of SUVs, respectively) plotted against residue number for WT aSyn and A30P (C) or WT aSyn and G51D (D). From these data we determined the fractional populations of exposed and hidden conformers for each variant (see Table 2). (E, F) Graphs showing values of $\{I/I_o\}_{A30P} - \{I/I_o\}_{WT}$ (E) or $\{I/I_o\}_{G51D} - \{I/I_o\}_{WT}$ (F) plotted against residue number. The data in (A)–(F) are representative of ≥2 experiments.

PG:PC vesicles (lipid:protein ratio, 20:1 mol/mol) at 37 °C for 72 or 96 h. The membrane fraction was isolated by lipid flotation (Fig. 4A) and examined by Western blotting. The lane loaded with the WT protein sample revealed a modest degree of laddering of aSyn immunoreactive bands at 37, 55, 80, and 100 kDa corresponding to SDS-resistant aggregates (Figs. 4B and C). Densitometry analysis of monomeric and oligomeric immunoreactive bands revealed a time-dependent increase in oligomerization between 72 and 96 h. The A30P and G51D variants, which both showed an increase in the proportion of exposed-state molecules in the NMR analysis, displayed more pronounced laddering and an increased overall accumulation of bands in the region of the gel corresponding to a molecular weight range of 55 to ~250 kDa. Densitometry analysis of the protein bands revealed that the mutants displayed an 85% and 115–140% increase in the ratio of higher molecular weight species to monomer relative to WT aSyn at 72 and 96 h, respectively (Figs. 4B and C). These results suggest that aSyn variants with an increased exposed-state population have a higher propensity to undergo membrane-induced aggregation.

Table 2
Fractional populations of membrane-bound aSyn conformers determined by NMR.

	Total bound[a,b]	Hidden[a,c]	Exposed[a,d]	Exposed relative to WT
WT	0.84	0.48	0.36	1.0
G51D	0.85	0.12	0.73	2.0
A30P	0.85	0.17	0.68	1.9
A29E	0.78	0.00	0.78	2.2
V49E	0.84	0.34	0.49	1.4

[a] Values were determined from ^{1}H–^{15}N-HSQC data in Figs. 3 and 7 and are expressed as a fraction of the total protein; each sample consisted of a mixture of aSyn and phospholipids at concentrations of 150 μM and 3 mM, respectively.
[b] Determined from the mean attenuation of residues 3–9 (i.e. total bound = 1 − $\{I/I_o\}_{mean,3-9}$).
[c] Determined from the mean attenuation of residues 66–80 (i.e. hidden = 1 − $\{I/I_o\}_{mean,66-80}$).
[d] Calculated as the difference between the total bound population and the hidden population.

The intensity of the monomer band in the vesicle fraction was greater in the case of A30P and G51D compared to WT aSyn (Figs. 4B and C). Because our CD data revealed a lower membrane affinity for both A30P and G51D compared to the WT protein (Table 1), we infer that the increased monomer immunoreactivity observed for the mutants must not reflect a greater degree of direct lipid binding. Instead, we interpret these results to mean that unbound monomer is recruited from the bulk solution into membrane-bound aggregates via a seeding mechanism, and thus A30P and G51D samples have a greater protein load at the membrane because they undergo more extensive membrane-induced aggregation. Any recruited monomer bound to membrane-

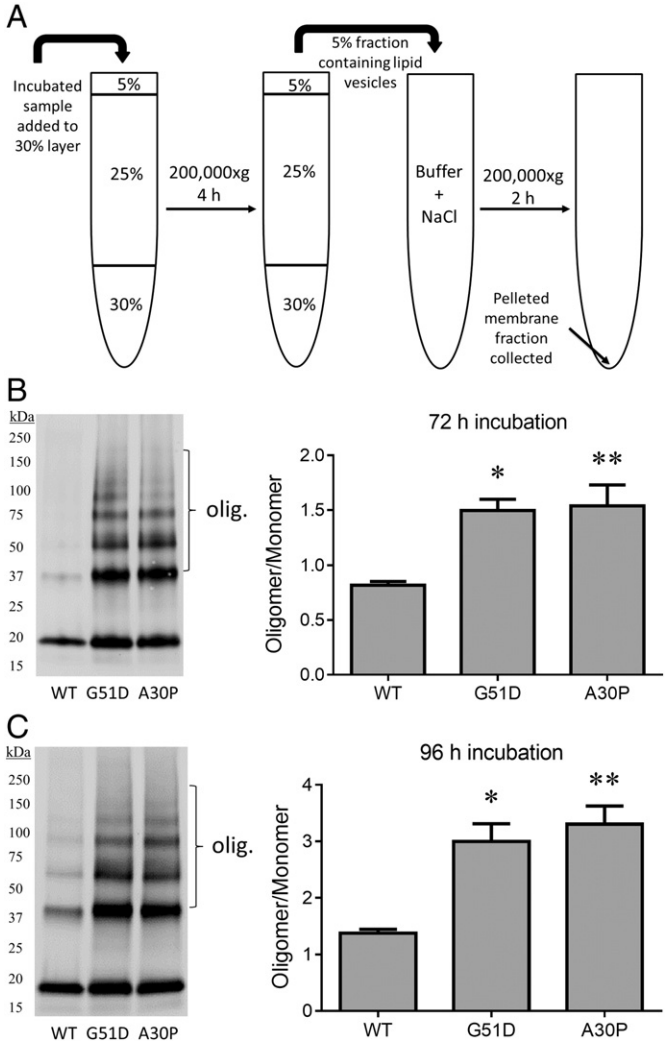

Fig. 4. A30P and G51D have a greater propensity to undergo membrane-induced aggregation compared to WT aSyn. (A) Schematic diagram of the lipid flotation method used to isolate the membrane fraction from an incubated mixture of aSyn and SUVs. (B, C) Results of Western blot analysis of membrane fractions obtained from aSyn/SUV mixtures incubated for 72 h (B) or 96 h (C). Left: Western blot images ('olig' refers to the region of the blot with bands corresponding to high molecular weight forms of aSyn). Right: Bar graphs showing the ratio of total oligomer band intensity to monomer band intensity determined for each sample via densitometric analysis. The data are presented as the mean ± SEM, n = 3; $^{*}p < 0.05$, $^{**}p < 0.01$, one-way ANOVA followed by Tukey's multiple comparisons post hoc test.

associated oligomers via non-covalent interactions would be expected to migrate as the monomeric form under the denaturing conditions of SDS-PAGE. Consistent with this interpretation, analysis of membrane fractions obtained after incubating WT aSyn, A30P, or G51D with SUVs for 2 h at 22 °C (a time sufficient for aSyn-lipid binding but not membrane-induced aggregation) revealed similar monomer band intensities for all three variants (data not shown).

Neurotoxicity of A30P and G51D

We examined whether differences in the propensities of WT aSyn, A30P, and G51D to undergo membrane-induced self-assembly correlated with differences in neurotoxicity. To address this question, we characterized the three aSyn variants in terms of their ability to elicit dopaminergic cell death and neurite retraction in a cell culture model consisting of primary midbrain cultures transduced with aSyn-encoding adenovirus. In an initial control experiment, cultures transduced with an adenovirus encoding EGFP downstream of the neuron-specific synapsin promoter were stained for microtubule associated protein 2 (MAP2), a general neuronal marker, or tyrosine hydroxylase (TH), a marker of dopaminergic neurons, and scored for the number of $MAP2^+$ or TH^+ neurons that expressed EGFP (Supplementary Fig. S2). From this analysis, we determined that the viral transduction efficiency was >90% for both $MAP2^+$ and TH^+ neurons. Next, primary midbrain cultures were transduced with adenoviruses encoding WT aSyn, A30P, or G51D at MOIs selected to ensure equal expression of all three variants (Supplementary Fig. S3) and stained for MAP2 and TH. Relative dopaminergic cell viability was evaluated by determining the percentage of $MAP2^+$ neurons that were also TH^+. We found that cultures expressing WT aSyn did not display a significant loss of dopaminergic neurons relative to an untreated control or a transduction control treated with LacZ virus (Fig. 5A; Supplementary Fig. S4A). In contrast, a significant reduction in the relative number of dopaminergic neurons was observed in cultures expressing A30P (Fig. 5A) or G51D (Figs. 5A and B; Supplementary Fig. S4A). Similar degrees of dopaminergic cell death were observed in cultures expressing A30P, G51D, or another familial PD mutant, A53T. Further analysis of the same cultures revealed a non-significant trend towards a decrease in the lengths of neurites extending from $MAP2^+/TH^+$ neurons in cultures expressing WT aSyn compared to cultures that were untreated or transduced with LacZ virus (Fig. 5C; Supplementary Fig. S4B). Cultures expressing A30P, G51D, or A53T displayed a marked reduction in TH^+ neurite lengths compared to control cultures or cultures expressing β-galactosidase or WT aSyn (Figs. 5C–E; Supplementary Fig. S4B). Because neurite lengths were measured by examining the MAP2 stain, these results suggest that the aSyn-mediated loss of TH^+ neurons shown in Figs. 5A and B and Supplementary Fig. S4A reflects a decrease in dopaminergic cell viability rather than just a reduction in TH expression. There were no significant differences in the lengths of neurites extending from $MAP2^+/TH^-$ neurons in cultures expressing any of the aSyn variants compared to cultures that were untreated or transduced with LacZ virus (Supplementary Fig. S5), strongly suggesting that aSyn expression was preferentially toxic to dopaminergic neurons in our model. Together, our findings suggest that aSyn variants with a higher propensity to undergo membrane-induced aggregation also display increased toxicity to primary dopaminergic neurons.

Effects of the A29E and V49E substitutions on aSyn–membrane interactions and membrane-induced aSyn aggregation

The results outlined above revealed that the G51D substitution interferes with aSyn–membrane interactions involving the central hydrophobic region, promotes membrane-induced aSyn aggregation, and enhances aSyn neurotoxicity. Our next objective was to determine the effects of introducing a negative charge at different sites on the amphipathic α11/3 helix of membrane-bound aSyn relative to the G51D mutation. We chose to focus on two mutations, A29E and V49E, because they were previously found to disrupt aSyn–membrane interactions in yeast and in a cell-free system (Volles and Lansbury, 2007). The glutamate residue of A29E is predicted to be in a similar position on the amphipathic α11/3 helix (relative to the lysine boundary separating the hydrophobic and hydrophilic faces) as the aspartate residue of G51D, though closer to the N-terminus (Fig. 1B). Because this part of the helix is thought to be embedded in the membrane, we predicted that the A29E substitution would disrupt membrane interactions similar to A30P and G51D. In contrast, the glutamate residue of V49E is predicted to be located on the aqueous side of the membrane interface, less in contact with the membrane. Accordingly, we predicted that the V49E substitution would perturb aSyn–membrane interactions to a lesser extent than A29E, A30P, or G51D.

Using the far-UV CD method described above, we first examined the degree of α-helicity of A29E and V49E relative to WT aSyn in the presence of increasing amounts of PG:PC and DOPE:DOPS:DOPC lipid vesicles. The lipid titration curves obtained for A29E and V49E in the

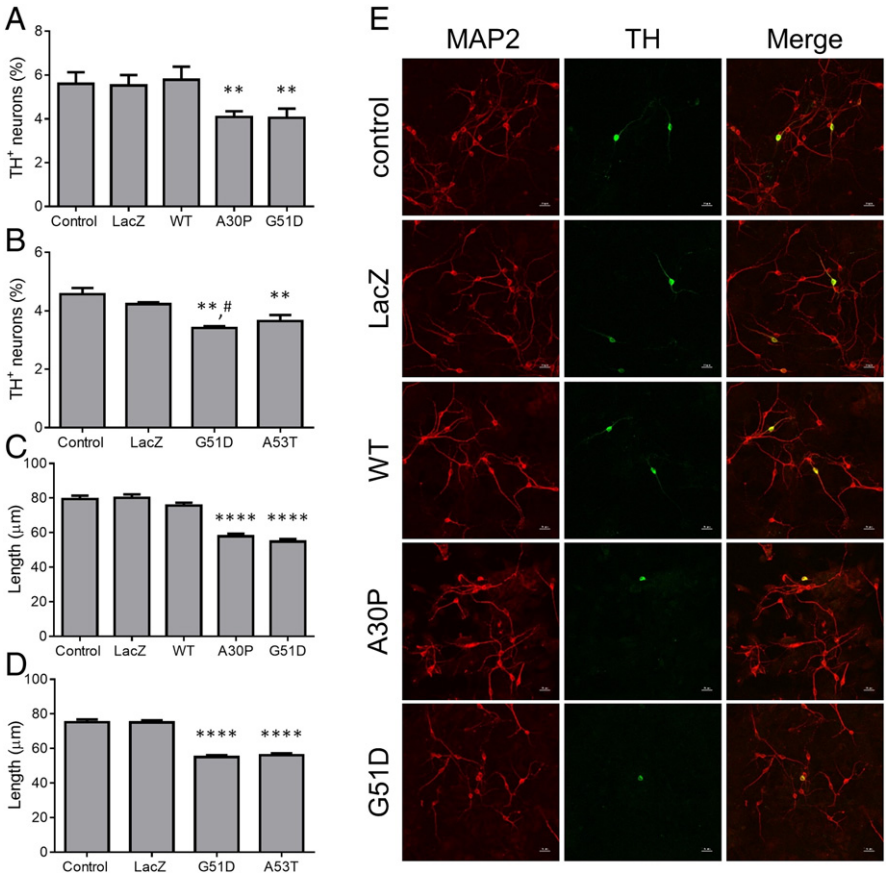

Fig. 5. A30P and G51D display enhanced neurotoxicity compared to WT aSyn. Primary midbrain cultures were transduced with adenoviruses encoding WT aSyn, A30P, and G51D (A, C) or G51D and A53T (B, D) at MOIs adjusted to ensure equal expression levels. Additional cultures were untransduced ('control') or transduced with LacZ adenovirus. The cells were fixed, stained with antibodies specific for MAP2 and TH, and scored for dopaminergic cell viability (A, B) or neurite lengths (C, D). The data are presented as the mean ± SEM, n = 4. (A, B) $^{**}p < 0.01$ versus control, LacZ, or WT (A); $^{**}p < 0.01$ versus control, $^{\#}p < 0.05$ versus LacZ (B); square root transformation, one-way ANOVA followed by Tukey's multiple comparisons post hoc test. (C, D) $^{****}p < 0.0001$ versus control, LacZ, or WT (C) or versus control or LacZ (D), Tukey's multiple comparisons post hoc test after general linear model implementation. (E) Representative fluorescence micrographs showing the more pronounced retraction of neurites extending from $MAP2^+/TH^+$ neurons in cultures expressing A30P or G51D compared to control cultures or cultures expressing β-galactosidase or WT aSyn (scale bar, 20 μm).

presence of PG:PC vesicles were significantly shifted to the right (with greater K_d values; $K_d = 7.5 \pm 0.7$ μM for A29E and 2.5 ± 0.4 for V49E) compared to the WT aSyn curve (Fig. 6A, Table 1). The degree of the rightward curve shift was greater for A29E than for V49E, and both variants displayed similar α-helical contents at saturating lipid concentrations compared to the WT protein. Similar results were observed for the three aSyn variants in the presence of DOPE:DOPS:DOPC vesicles ($K_d = 5 \pm 1$ μM for A29E and 1.8 ± 0.4 for V49E) (Fig. 6B, Table 1). Collectively, these data indicate that (i) A29E and (to a lesser extent) V49E have a reduced affinity for PG:PC and DOPE:DOPS:DOPC vesicles compared to WT aSyn; and (ii) the α-helical content of A29E and V49E is similar to that of the WT protein in the presence of saturating lipid.

Next, we investigated the membrane-bound conformation of the A29E and V49E variants via 2D NMR spectroscopy. ^{15}N-labeled forms of these mutants were incubated with or without DOPE:DOPS:DOPC vesicles (lipid:protein ratio, 20:1 mol/mol), and ^{1}H–^{15}N HSQC spectra were recorded (Figs. 7A and B). We found that A29E displayed a slight reduction in the total bound population and exhibited the greatest

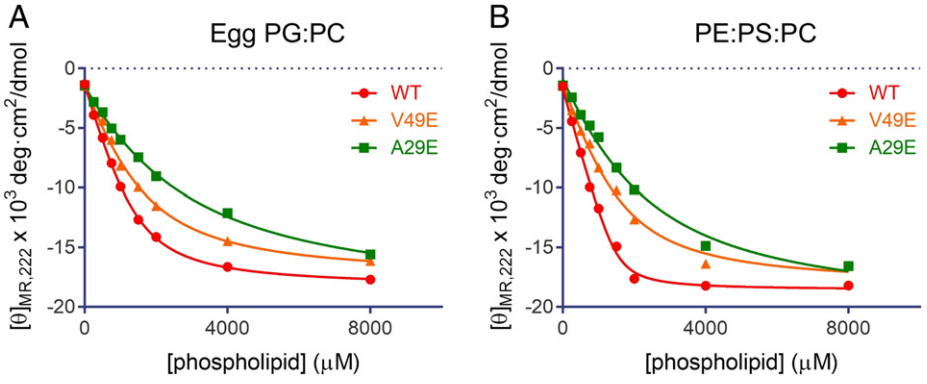

Fig. 6. A29E and V49E display reduced membrane affinity relative to WT aSyn. Solutions of recombinant aSyn variants were analyzed by far-UV CD as in Fig. 2. Each aSyn variant was incubated with increasing concentrations of SUVs composed of egg PG:PC (A) or DOPE:DOPS:DOPC (B) (the data for WT aSyn are identical to those presented in Fig. 2). The data were fit to Eq. (2), and values for K_d, minimum $[\theta]_{MR,\,222}$, and maximum α-helical content were determined from the values of the fit parameters (see Table 1). The data are representative of ≥3 experiments (in total, including both lipid compositions).

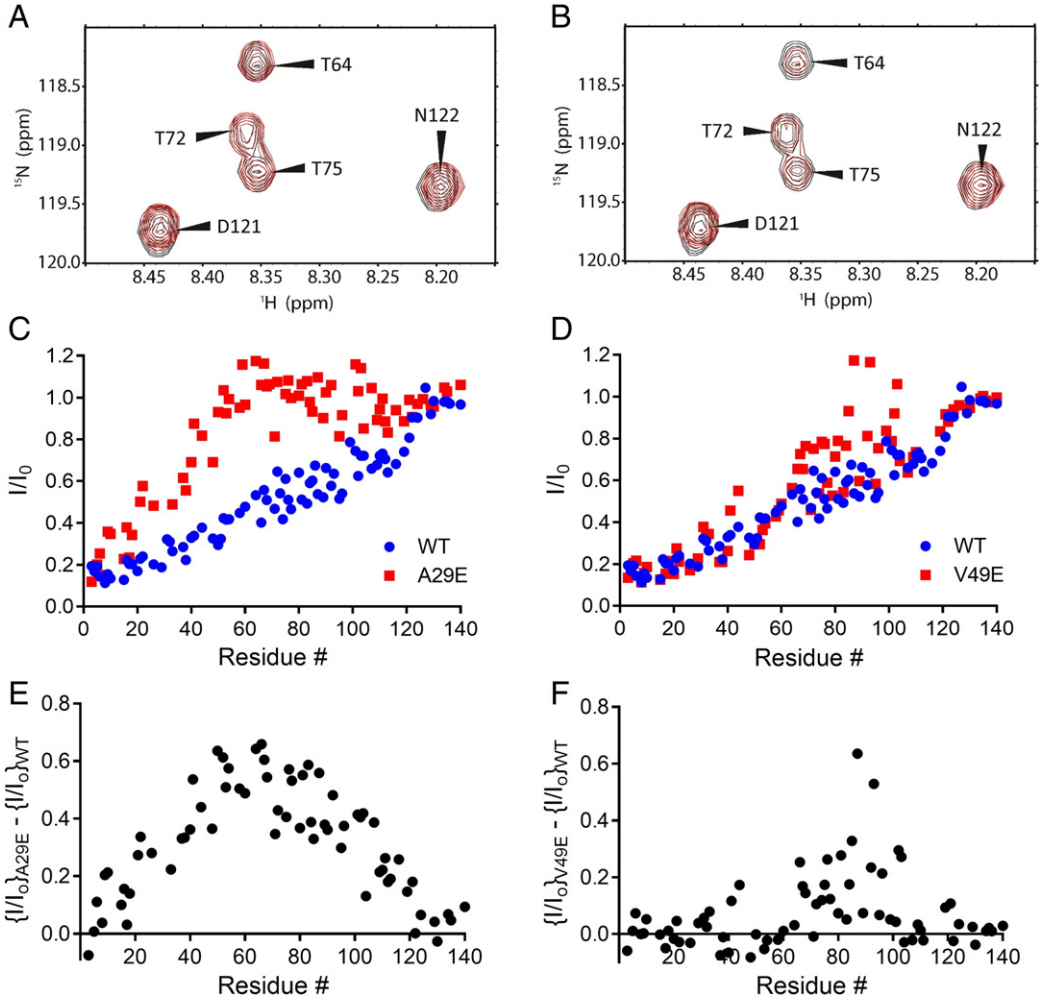

Fig. 7. A29E and to a lesser extent V49E have a greater propensity to adopt an exposed membrane-bound conformation than WT aSyn. ^{15}N-labeled aSyn variants were incubated with or without DOPE:DOPS:DOPC SUVs (lipid:protein ratio, 20:1 mol/mol) and analyzed by 2D NMR. (A, B) Selected region of the ^{1}H–^{15}N HSQC spectrum of A29E (A) or V49E (B) in the absence (black) or presence (red) of SUVs. (C, D) Graphs of I/I_0 (defined in Fig. 3) plotted against residue number for WT aSyn and A29E (C) or WT aSyn and V49E (D) (the data for WT aSyn are identical to those presented in Fig. 3). From these data we determined the fractional populations of exposed and hidden conformers for each variant (see Table 2). (E, F) Graphs showing values of $\{I/I_o\}_{A29E} - \{I/I_o\}_{WT}$ (E) or $\{I/I_o\}_{V49E} - \{I/I_o\}_{WT}$ (F) plotted against residue number. The data in (A)–(F) are representative of ≥2 experiments.

percentage of molecules in the exposed state of all the aSyn variants examined in this study, with ~78% of the total protein populating this state (corresponding to a 2.2-fold increase relative to WT aSyn) (Fig. 7C, Table 2). In contrast, only 49% of total V49E molecules were found to populate the exposed state, corresponding to a 1.4-fold increase over the WT protein (Fig. 7D, Table 2). Examination of the sequence dependence of the NMR signal attenuation from N- to C-terminus revealed that the decrease in attenuation exhibited by A29E

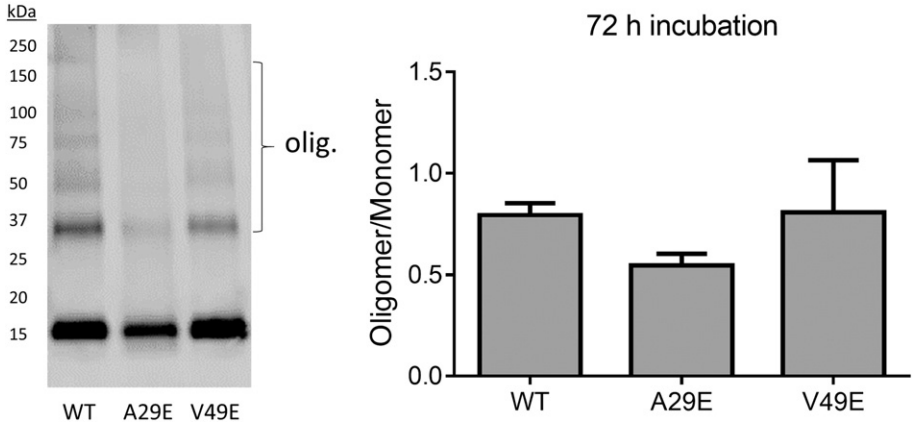

Fig. 8. A29E and V49E do not have a greater propensity to undergo membrane-induced aggregation compared to WT aSyn. Membrane fractions obtained from aSyn/SUV mixtures incubated for 72 h were analyzed via Western blotting. Left: Western blot image ('olig' refers to the region of the blot with bands corresponding to high molecular weight forms of aSyn). Right: Bar graph showing the ratio of total oligomer band intensity to monomer band intensity determined for each sample via densitometric analysis. The data are presented as the mean ± SEM, n = 3.

relative to WT aSyn began in the region of the amino acid substitution, whereas a similar lifting off effect was not apparent in the case of V49E, and the average magnitude of the attenuation decrease observed for this variant was substantially lower (Figs. 7E and F). These results suggest that the A29E substitution interferes with aSyn–membrane contacts, thereby favoring the exposed conformation, whereas the V49E substitution has a less disruptive effect on aSyn–membrane interactions.

To examine the effects of the A29E and V49E mutations on the ability of aSyn to undergo membrane-induced aggregation, we incubated each aSyn variant with PG:PC vesicles at 37 °C for 72 h, and membrane fractions isolated by lipid flotation were analyzed via Western blotting. The data revealed a trend towards a decrease in the oligomer/monomer ratio for A29E, and no difference in the oligomer/monomer ratio for V49E, compared to WT aSyn (Fig. 8). These results indicate that A29E and V49E do not have an increased ability to undergo membrane-induced aggregation compared to the WT protein despite having a greater propensity to adopt an exposed conformation at the membrane surface.

Effects of the A29E and V49E substitutions on aSyn neurotoxicity

Lastly, we examined the effects of the A29E and V49E substitutions on aSyn neurotoxicity. Primary midbrain cultures transduced with adenovirus encoding WT aSyn, A29E, or V49E were co-stained for TH and MAP2 and scored for relative dopaminergic cell viability. In this set of experiments, we found that cultures expressing WT aSyn displayed either (i) a modest loss of dopaminergic neurons compared to untreated control cultures, but not compared to cultures transduced with LacZ virus (Fig. 9A); or (ii) no loss of dopaminergic neurons compared to untreated or β-galactosidase expressing cultures (Fig. 9B). Our observation that WT aSyn exhibited variable levels of neurotoxicity (or trends towards a neurotoxic effect) in different experiments reflects normal variation inherent to the use of this primary cell culture model, coupled with the reduced neurotoxicity of the WT protein compared to the familial aSyn mutants, and is consistent with our evidence that WT aSyn-expressing cultures exhibit a non-significant trend towards a decrease in the lengths of neurites extending from $TH^+/MAP2^+$ neurons (Fig. 5C; Supplementary Fig. S4B). A53T-expressing cultures exhibited a significant loss of dopaminergic neurons compared to untreated control cultures and cultures transduced with LacZ virus (Figs. 9A and B). In contrast, cultures expressing A29E or V49E displayed no reduction in the relative number of dopaminergic neurons compared to untreated cultures or cultures transduced with virus encoding β-galactosidase or WT aSyn. These results suggest that A29E and V49E, two variants with an increased propensity to adopt an exposed, membrane-bound conformation but a weak ability to undergo membrane-induced aggregation compared to WT aSyn, are relatively non-toxic to primary dopaminergic neurons.

Discussion

Identifying aSyn conformers that produce neurotoxic aggregates is a major priority in the PD field, as these species could be potential therapeutic targets. In this effort, many studies have been carried out to characterize aSyn fibrillization in solution but have failed to consistently correlate fibrillization with toxicity (Rutherford et al., 2014; Volles and Lansbury, 2007). In addition, drug discovery efforts have been aimed at identifying small molecule inhibitors of aSyn fibrillization in solution (Ehrnhoefer et al., 2008; Masuda et al., 2006; Ono and Yamada, 2006), yet some reports from clinical trials suggest that this approach may not be effective (Low et al., 2014). Here, we used a different approach of examining aSyn self-assembly at the surface of phospholipid membranes, and we investigated how this phenomenon relates to aSyn neurotoxicity. Our study involved the use of a combination of approaches that enabled us to monitor membrane affinity, aSyn conformation, membrane-induced aSyn aggregation, and aSyn neurotoxicity. By analyzing a carefully chosen set of aSyn variants with different effects on these parameters, we obtained unique insights into molecular mechanisms by which aSyn could form neurotoxic oligomers at the membrane surface.

Disruption of contacts between the non-polar face of α-helical aSyn and the phospholipid bilayer favors a conformation of membrane-bound aSyn with greater exposure of the central hydrophobic region

A number of groups have proposed that reduced membrane interactions in the central hydrophobic region promote aSyn aggregation at the membrane surface (Bartels et al., 2010; Bodner et al., 2009, 2010; Dikiy and Eliezer, 2012; Mazumder et al., 2013). To examine this hypothesis, we characterized the aSyn mutants A29E, A30P, V49E, and G51D in terms of their membrane interactions and propensity to undergo membrane-induced aggregation. These mutants were chosen based on the prediction that their amino acid substitutions would disrupt aSyn–phospholipid contacts at various positions on the amphipathic α11/3 helix (Fig. 1B). All four mutants exhibited reduced affinity for SUVs with two different phospholipid compositions compared to WT aSyn, although the membrane affinities of A29E and G51D were less than those of A30P and V49E. These results are consistent with previous data suggesting that A30P has reduced membrane affinity (Jensen et al., 1998; Jo et al., 2002; Perrin et al., 2000) and with the following, previously reported rank order of membrane affinities (Volles and Lansbury, 2007): A29E ≈ A30P < V49E < WT aSyn. Although one group reported that G51D adopted a similar degree of α-helical structure compared to WT aSyn in the presence of DOPG

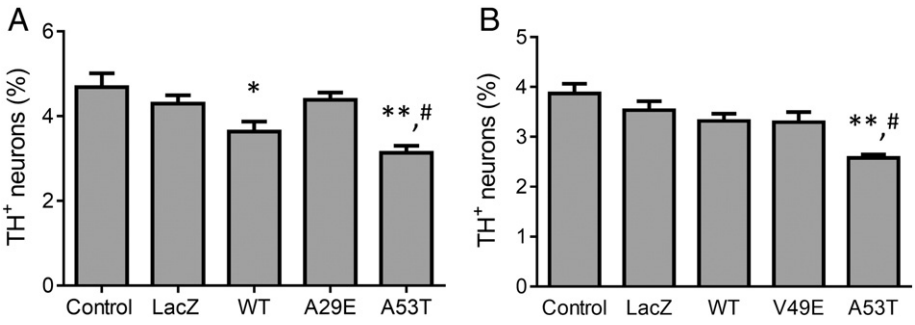

Fig. 9. A29E and V49E do not exhibit enhanced neurotoxicity compared to WT aSyn. Primary midbrain cultures were transduced with adenoviruses encoding WT aSyn, A53T, and A29E (A) or WT aSyn, A53T, and V49E (B) at MOIs adjusted to ensure equal expression levels. Additional cultures were untransduced ('control') or transduced with LacZ adenovirus. The cells were fixed, stained with antibodies specific for MAP2 and TH, and scored for dopaminergic cell viability. The data are presented as the mean ± SEM, n = 3–6; $^*p < 0.05$, $^{**}p < 0.01$ versus control, $^{\#}p < 0.05$ versus LacZ, square root transformation, one-way ANOVA, followed by Tukey's multiple comparisons post hoc test.

vesicles (Lesage et al., 2013), a recent study revealed that G51D has reduced affinity for 1-palmitoyl-2-oleoyl-*sn*-glycero-3-phosphoglycerol (POPG) SUVs compared to the WT protein (Fares et al., 2014), in support of the findings reported here.

Our observation that G51D has a reduced maximum helicity compared to A29E or A30P is likely a result of the more C-terminal position of the G51D mutation in the α11/3 helix compared to the other two substitutions. The aSyn region spanning residues 31–85 has been reported to have lower membrane affinity than the N-terminal segment spanning the first ~30 residues (Bartels et al., 2010; Drescher et al., 2008; Shvadchak et al., 2011b). Interactions involving residues 31–85 with the membrane only become significant after the crowding of neighboring aSyn molecules on the bilayer surface is relieved by the addition of excess lipid. Apparently, attractive forces between this segment of aSyn and the membrane can overcome the disruptive effects of the A29E and A30P mutations in the presence of saturating lipid. In contrast, the summed attractive forces between residues C-terminal to the G51D substitution and the membrane may be too weak to overcome the disruptive effects of this mutation, resulting in a loss of binding of this region even in the presence of excess lipid.

Analysis of aSyn–membrane interactions by 2D NMR enabled us to identify residue-specific interactions that were disrupted by amino acid substitutions in the aSyn variants. We found that all four mutants exhibited similar fractional populations of membrane-bound molecules – defined as molecules with the segment spanning residues 3–9 in contact with the membrane – compared to the WT protein under the conditions of the NMR experiment (incubation with DOPE:DOPS:DOPC SUVs at a protein:lipid ratio of 1:20). NMR data obtained for the familial mutants A30P and G51D revealed a marked disruption of membrane interactions that started near the site of the mutation and extended through the C-terminal end of the α11/3 helix. These findings are consistent with 2D NMR data obtained for A30P (Bodner et al., 2010) and with NMR results reported for G51D while this manuscript was in preparation (Fares et al., 2014). Our 2D NMR analysis of A29E revealed a disruption of membrane contacts that began near the site of the mutation and extended into the C-terminal region. In contrast, V49E exhibited more modest perturbations of membrane contacts compared to A29E, A30P, and G51D.

Examination of a helical wheel plot sheds light on possible mechanisms by which aSyn–membrane interactions could be disrupted by different mutations. Although the A29E and A30P substitutions occur at adjacent positions in the aSyn sequence, the mechanisms by which they disrupt membrane binding are different. Introduction of a helix-breaking proline residue at position 30 reduces the membrane affinity of aSyn by destabilizing the α11/3 helix that plays a key role in membrane binding (Jensen et al., 1998; Jo et al., 2002; Perrin et al., 2000). In contrast, the A29E substitution introduces a negatively charged glutamate residue at a site on the non-polar face of the α11/3 helix that is predicted to be embedded in the hydrophobic (acyl chain) region of the phospholipid bilayer. The A29E mutation shows more extensive disruption of contacts (and weaker affinity observed by far-UV CD) compared to A30P, presumably because of the higher energy barrier associated with introducing a negative charge in the non-polar phase of the bilayer. Residues A29 and G51 are aligned equivalently (i.e. they have the same angular position) on the helical wheel plot of WT aSyn (Fig. 1B). Thus, the G51D substitution would be expected to have a similar disruptive effect on membrane binding as the A29E mutation because of the high energy barrier associated with inserting a charged aspartate residue in the hydrophobic region of the bilayer. Consistent with this prediction, both G51D and A29E bind SUVs with weaker affinity (based on far-UV CD data) compared to WT aSyn, although as expected the A29E substitution disrupts membrane contacts at more N-terminal sites compared to the G51D substitution. Although V49 is only two residues N-terminal to G51 in the amino acid sequence, the V49E substitution has a less disruptive effect on membrane interactions and affinity than the G51D mutation, presumably because V49 is situated on the polar face of the amphipathic helix at a site that is expected to be near the protein–membrane interface. Thus, the glutamate residue at position 49 of V49E should not be involved in destabilizing interactions with the non-polar phase of the bilayer. Instead, it could engage in repulsive electrostatic interactions with anionic phospholipid head-groups, perhaps via a mechanism involving partial helix unfolding (Pandey et al., 2009).

Collectively, our findings highlight the fact that the degree of exposure of a membrane-bound aSyn variant with a mutation encoding a charged residue depends on the placement of the residue on the amphipathic α11/3 helix relative to the membrane contact region. Disruption of contacts between the non-polar face of the helix and the hydrophobic region of the bilayer results in the protein's adoption of an exposed conformation. Moreover, the introduction of a charged residue at a more N-terminal site on the non-polar face of the helix results in a more extensive disruption of aSyn–membrane interactions.

The adoption of an exposed conformation by membrane-bound aSyn can promote (but is not sufficient for) membrane-induced aggregation

Based on the hypothesis that exposure of the central hydrophobic region of membrane-bound aSyn favors aSyn aggregation at the membrane surface (Bartels et al., 2010; Bodner et al., 2009, 2010; Dikiy and Eliezer, 2012; Mazumder et al., 2013), one would predict that A30P, G51D, and A29E, which adopt a relatively exposed conformation in the membrane-bound state, should have a higher propensity to undergo membrane-induced aggregation compared to the WT protein. Conversely, the V49E mutant, which has a lower tendency to adopt an exposed conformation compared to A30P, G51D, and A29E, should have a reduced ability to undergo self-assembly at the membrane surface compared to the other three mutants. In partial agreement with this prediction, A30P and G51D both display significantly increased aggregation relative to WT aSyn upon incubation in the presence of SUVs, whereas V49E exhibits less membrane-induced self-assembly compared to the two familial mutants. To our knowledge, these data provide the first direct evidence that A30P and G51D undergo enhanced membrane-induced aggregation upon prolonged incubation with SUVs. During the preparation of this manuscript, it was reported that G51D converts from an α-helical structure to a β-sheet-rich structure when incubated with SUVs (Fares et al., 2014), implying that the oligomers formed in the G51D–lipid mixtures described here have considerable β-sheet structure.

In contrast, the results obtained with A29E do not support the hypothesis that the exposed conformation of membrane-bound aSyn invariably favors membrane-induced aggregation. Although A29E is similar to G51D in terms of its placement of a negatively charged residue on the non-polar face of the α11/3 helix and the degree to which it adopts an exposed conformation, it does not have the same high propensity to undergo oligomerization in the presence of SUVs. Two explanations could account for this finding. First, the length of the N-terminal α11/3 helix adopted by membrane-bound A29E may be insufficient to enable interactions between neighboring aSyn molecules required for self-assembly on the bilayer. However, the fact that the N-terminal helix formed by A29E encompasses a similar number of residues compared to the A30P N-terminal helix (~20 residues in both cases) and that A30P (in contrast to A29E) has a high propensity to undergo membrane-induced aggregation is inconsistent with this explanation. Second, the glutamate residue at position 29 of neighboring, membrane-bound A29E molecules may engage in repulsive electrostatic interactions that interfere with self-assembly on the bilayer. This scenario implies that the introduction of a negative charge at position 29 electrostatically interferes with self-assembly, whereas the G51D substitution does not have the same inhibitory effect, perhaps because contacts involving residue 51 do not play a significant role in aSyn oligomerization on the membrane surface. Consistent with this model,

evidence suggests that aSyn forms oligomers on the membrane surface via interactions between the α-helical domains of neighboring protein molecules, and in particular, via parallel interactions involving the helical segment spanning residues ~1–40 (Burre et al., 2014). Although membrane-bound helical aSyn oligomers apparently play a role in the physiologically relevant binding of the protein to synaptobrevin (Burre et al., 2014), they could also be precursors of pathological, β-sheet-rich aggregates that form on the membrane as a result of exposure of the central hydrophobic region (Comellas et al., 2012; Mazumder et al., 2013; Pandey et al., 2009).

Together, our observations indicate that the potential impact of a mutation on aSyn self-assembly at the membrane surface is more complex than previously suggested. Namely, the effect of a mutation on the propensity of aSyn to undergo membrane-induced aggregation depends not only on how the mutation alters the distribution of aSyn between exposed and hidden conformers, but also on how it affects interactions between membrane-bound aSyn molecules necessary for higher order assembly on the bilayer. In particular, our findings highlight the importance of contacts involving a segment of the polypeptide chain encompassing residue 29 for membrane-induced aSyn aggregation.

Membrane-induced aSyn aggregation may play a role in aSyn neurotoxicity

A key outcome of our study is the observation that the propensity of aSyn variants to undergo membrane-induced self-assembly correlates with their neurotoxicity. Both A30P and G51D displayed greater membrane-induced aggregation and enhanced toxicity to dopaminergic neurons compared to WT aSyn. In contrast, A29E displayed trends towards decreased membrane-induced self-assembly and reduced neurotoxicity. From these results, we infer that aSyn aggregation at the membrane surface could contribute to aSyn-mediated neurodegeneration in PD. This conclusion is supported by evidence that other neurotoxic aSyn variants, including A53T and the engineered mutant E57K (Reynolds et al., 2011) and a series of aSyn variants originally characterized in yeast (Vamvaca et al., 2009; Volles and Lansbury, 2007) (Griggs, A.M. and Rochet, J.-C., unpublished data), have an increased propensity to undergo membrane-induced self-assembly. In addition, we have obtained data showing that the familial aSyn mutants A53T and E46K both have a greater propensity to undergo membrane-induced aggregation and elicit neurotoxicity compared to WT aSyn (Griggs, A.M. and Rochet, J.-C., unpublished data). By analogy with mutations that disrupt aSyn-bilayer contacts, perturbations that favor a more exposed conformation of the membrane-bound WT protein, including aSyn oxidation (Maltsev et al., 2013) and changes in membrane lipid composition (Fusco et al., 2014), could contribute to aSyn aggregation and neurotoxicity in sporadic PD.

Multiple lines of evidence suggest that aSyn aggregation at the membrane surface results in a disruption of membrane integrity, apparently via a mechanism involving lipid extraction from the bilayer (Comellas et al., 2012; Lee et al., 2012; Ouberai et al., 2013; Reynolds et al., 2011). This process of bilayer disruption coupled to the aggregation of membrane-bound aSyn, and/or the formation of the aggregates themselves, could play a role in neurotoxic mechanisms associated with aSyn expression in cellular and animal models, including interference with cellular trafficking (Cooper et al., 2006; Gitler et al., 2008; Soper et al., 2011) or impairment of mitochondrial function or dynamics (Kamp et al., 2010; Nakamura et al., 2011; Parihar et al., 2009).

Although our results highlight a potential connection between membrane-induced aSyn aggregation and neurotoxicity, they do not exclude the possibility that aSyn triggers neurodegeneration via additional mechanisms, including oligomerization in solution rather than at the membrane surface (Burre et al., 2015). In the case of G51D, several groups have reported that the mutant protein undergoes oligomerization or fibrillization in solution with similar or slower kinetics compared to WT aSyn (Fares et al., 2014; Lesage et al., 2013; Rutherford et al., 2014). Thus, the enhanced neurotoxicity of G51D in familial PD patients can be explained by the mutant's high propensity to undergo membrane-induced self-assembly (shown here), as opposed to its relatively modest ability to form aggregates in solution. Our observation that G51D has reduced α-helical content in the presence of saturating phospholipid suggests that the protein could adopt an exposed conformation and form potentially toxic oligomers at the membrane surface at a range of protein–lipid ratios (e.g. resulting from variations in protein expression levels) in vivo. In contrast to G51D, evidence suggests that A30P has an enhanced ability to undergo oligomerization in solution (Conway et al., 2000; Li et al., 2001) and in the presence of SUVs (this study) relative to WT aSyn. Accordingly, the enhanced neurotoxicity of A30P in familial PD can be accounted for by both self-assembly mechanisms. A number of engineered aSyn mutants have been reported to have an increased ability to form oligomers in solution and to elicit neurodegeneration compared to WT aSyn (Karpinar et al., 2009; Winner et al., 2011). A goal for future research will be to determine whether membrane-induced aggregation could play a role in the enhanced neurotoxicity of these and other aSyn variants (Burre et al., 2012).

Conclusions

In summary, our data show that the A30P and G51D mutations reduce the membrane affinity of aSyn, leading to an increase in the fractional population of the exposed state. Upon incubation, these variants also display increased membrane-induced self-assembly relative to WT aSyn, and this property correlates with increased toxicity to dopaminergic neurons. Our observations support a model wherein the conformation of aSyn on phospholipid membranes plays a key role in initiating the formation of neurotoxic aggregates. However, an increase in the exposed state population is not itself sufficient for membrane-induced aggregation or neurotoxicity, as disrupting interactions between neighboring exposed conformers could impede the formation of toxic aggregates at the membrane surface. Collectively, our findings provide a rationale for alleviating aSyn neurotoxicity in PD and other synucleinopathy disorders by stabilizing aSyn–membrane interactions to favor the hidden state (Fonseca-Ornelas et al., 2014), or by interfering with the association of exposed conformers at the membrane surface.

Supplementary data to this article can be found online at http://dx.doi.org/10.1016/j.nbd.2015.04.007.

Acknowledgments

This work was supported by a grant from the Branfman Family Foundation (J.-C.R.), NIH grants R01 NS049221 (J.-C.R.), R01 GM039478 (C.B.P.), and K25 NS058395-04 (L.A.S.), a Purdue Research Foundation Fellowship (J.-C.R. and D.Y.), a McKeehan Fellowship provided by the College of Pharmacy at Purdue University (D.Y.), and a Floss Endowment Research Award provided by the Department of Medicinal Chemistry and Molecular Pharmacology at Purdue University (D.Y.). The research described herein was conducted in a facility constructed with support from Research Facilities Improvement Program grant nos. C06-14499 and C06-15480 from the National Center for Research Resources of the NIH. NMR data were acquired in the PINMRF supported by P30 CA023168. We thank Dr. Katherine Strathearn and Susan Roy for assistance with analyzing primary midbrain cultures, Dr. David Eliezer for providing NMR assignments for WT aSyn, Dr. Deniz Kirik for providing the pAAV2 plasmid, and Dr. Volodymyr Shvadchak for helpful suggestions for analyzing the data from far-UV CD experiments.

References

Abedini, A., Raleigh, D.P., 2009. A role for helical intermediates in amyloid formation by natively unfolded polypeptides? Phys. Biol. 6, 15005.

Bartels, T., et al., 2010. The N-terminus of the intrinsically disordered protein alpha-synuclein triggers membrane binding and helix folding. Biophys. J. 99, 2116–2124.

Bertoncini, C.W., et al., 2005. Release of long-range tertiary interactions potentiates aggregation of natively unstructured alpha-synuclein. Proc. Natl. Acad. Sci. U. S. A. 102, 1430–1435.
Bodner, C.R., et al., 2009. Multiple tight phospholipid-binding modes of alpha-synuclein revealed by solution NMR spectroscopy. J. Mol. Biol. 390, 775–790.
Bodner, C.R., et al., 2010. Differential phospholipid binding of alpha-synuclein variants implicated in Parkinson's disease revealed by solution NMR spectroscopy. Biochemistry 49, 862–871.
Burre, J., et al., 2012. Systematic mutagenesis of alpha-synuclein reveals distinct sequence requirements for physiological and pathological activities. J. Neurosci. 32, 15227–15242.
Burre, J., et al., 2014. alpha-Synuclein assembles into higher-order multimers upon membrane binding to promote SNARE complex formation. Proc. Natl. Acad. Sci. U. S. A. 111, E4274–E4283.
Burre, J., et al., 2015. Definition of a molecular pathway mediating alpha-synuclein neurotoxicity. J. Neurosci. 35, 5221–5232.
Bussell Jr., R., Eliezer, D., 2003. A structural and functional role for 11-mer repeats in α-synuclein and other exchangeable lipid binding proteins. J. Mol. Biol. 329, 763–778.
Chandra, S., et al., 2003. A broken α-helix in folded α-synuclein. J. Biol. Chem. 278, 15313–15318.
Chartier-Harlin, M.C., et al., 2004. Alpha-synuclein locus duplication as a cause of familial Parkinson's disease. Lancet 364, 1167–1169.
Comellas, G., et al., 2012. Structural intermediates during alpha-synuclein fibrillogenesis on phospholipid vesicles. J. Am. Chem. Soc. 134, 5090–5099.
Conway, K.A., et al., 2000. Acceleration of oligomerization, not fibrillization, is a shared property of both α-synuclein mutations linked to early-onset Parkinson's disease: implications for pathogenesis and therapy. Proc. Natl. Acad. Sci. U. S. A. 97, 571–576.
Cooper, A.A., et al., 2006. Alpha-synuclein blocks ER–Golgi traffic and Rab1 rescues neuron loss in Parkinson's models. Science 313, 324–328.
Davidson, W.S., et al., 1998. Stabilization of α-synuclein secondary structure upon binding to synthetic membranes. J. Biol. Chem. 273, 9443–9449.
Dedmon, M.M., et al., 2005. Mapping long-range interactions in alpha-synuclein using spin-label NMR and ensemble molecular dynamics simulations. J. Am. Chem. Soc. 127, 476–477.
Delaglio, F., et al., 1995. NMRPipe: a multidimensional spectral processing system based on UNIX pipes. J. Biomol. NMR 6, 277–293.
Dikiy, I., Eliezer, D., 2012. Folding and misfolding of alpha-synuclein on membranes. Biochim. Biophys. Acta 1818, 1013–1018.
Drescher, M., et al., 2008. Spin-label EPR on alpha-synuclein reveals differences in the membrane binding affinity of the two antiparallel helices. Chembiochem 9, 2411–2416.
Ehrnhoefer, D.E., et al., 2008. EGCG redirects amyloidogenic polypeptides into unstructured, off-pathway oligomers. Nat. Struct. Mol. Biol. 15, 558–566.
Eliezer, D., et al., 2001. Conformational properties of α-synuclein in its free and lipid-associated states. J. Mol. Biol. 307, 1061–1073.
Fares, M.B., et al., 2014. The novel Parkinson's disease linked mutation G51D attenuates in vitro aggregation and membrane binding of alpha-synuclein, and enhances its secretion and nuclear localization in cells. Hum. Mol. Genet. 23, 4491–4509.
Ferreon, A.C., et al., 2009. Interplay of alpha-synuclein binding and conformational switching probed by single-molecule fluorescence. Proc. Natl. Acad. Sci. U. S. A. 106, 5645–5650.
Fonseca-Ornelas, L., et al., 2014. Small molecule-mediated stabilization of vesicle-associated helical alpha-synuclein inhibits pathogenic misfolding and aggregation. Nat. Commun. 5, 5857.
Fusco, G., et al., 2014. Direct observation of the three regions in alpha-synuclein that determine its membrane-bound behaviour. Nat. Commun. 5, 3827.
Galvagnion, C., et al., 2015. Lipid vesicles trigger alpha-synuclein aggregation by stimulating primary nucleation. Nat. Chem. Biol. 11, 229–234.
Georgieva, E.R., et al., 2010. The lipid-binding domain of wild type and mutant alpha-synuclein: compactness and interconversion between the broken and extended helix forms. J. Biol. Chem. 285, 28261–28274.
Giasson, B.I., et al., 2001. A hydrophobic stretch of 12 amino acid residues in the middle of α-synuclein is essential for filament assembly. J. Biol. Chem. 276, 2380–2386.
Giehm, L., et al., 2010. SDS-induced fibrillation of alpha-synuclein: an alternative fibrillation pathway. J. Mol. Biol. 401, 115–133.
Gitler, A.D., et al., 2008. The Parkinson's disease protein alpha-synuclein disrupts cellular Rab homeostasis. Proc. Natl. Acad. Sci. U. S. A. 105, 145–150.
Greenbaum, E.A., et al., 2005. The E46K mutation in alpha-synuclein increases amyloid fibril formation. J. Biol. Chem. 280, 7800–7807.
Grey, M., et al., 2015. Acceleration of alpha-synuclein aggregation by exosomes. J. Biol. Chem. 290, 2969–2982.
Haque, F., et al., 2010. Adsorption of alpha-synuclein on lipid bilayers: modulating the structure and stability of protein assemblies. J. Phys. Chem. B 114, 4070–4081.
Jao, C.C., et al., 2004. Structure of membrane-bound alpha-synuclein studied by site-directed spin labeling. Proc. Natl. Acad. Sci. U. S. A. 101, 8331–8336.
Jensen, P.H., et al., 1998. Binding of α-synuclein to brain vesicles is abolished by familial Parkinson's disease mutation. J. Biol. Chem. 273, 26292–26294.
Jo, E., et al., 2000. α-Synuclein membrane interactions and lipid specificity. J. Biol. Chem. 275, 34328–34334.
Jo, E., et al., 2002. Defective membrane interactions of familial Parkinson's disease mutant A30P α-synuclein. J. Mol. Biol. 315, 799–807.
Jo, E., et al., 2004. alpha-Synuclein-synaptosomal membrane interactions: implications for fibrillogenesis. Eur. J. Biochem. 271, 3180–3189.
Kamp, F., et al., 2010. Inhibition of mitochondrial fusion by alpha-synuclein is rescued by PINK1, Parkin and DJ-1. Embo J. 29, 3571–3589.
Karpinar, D.P., et al., 2009. Pre-fibrillar alpha-synuclein variants with impaired beta-structure increase neurotoxicity in Parkinson's disease models. Embo J. 28, 3256–3268.
Kiely, A.P., et al., 2013. alpha-Synucleinopathy associated with G51D SNCA mutation: a link between Parkinson's disease and multiple system atrophy? Acta Neuropathol. 125, 753–769.
Kruger, R., et al., 1998. Ala30Pro mutation in the gene encoding α-synuclein in Parkinson's disease. Nat. Genet. 18, 106–108.
Lee, H.-J., et al., 2002. Membrane-bound α-synuclein has a high aggregation propensity and the ability to seed the aggregation of the cytosolic form. J. Biol. Chem. 277, 671–678.
Lee, J.H., et al., 2012. Radiating amyloid fibril formation on the surface of lipid membranes through unit-assembly of oligomeric species of alpha-synuclein. PLoS ONE 7, e47580.
Lesage, S., et al., 2013. G51D alpha-synuclein mutation causes a novel parkinsonian-pyramidal syndrome. Ann. Neurol. 73, 459–471.
Li, J., et al., 2001. Effect of familial Parkinson's disease point mutations A30P and A53T on the structural properties, aggregation, and fibrillation of human α-synuclein. Biochemistry 40, 11604–11613.
Liu, F., et al., 2008. Methionine sulfoxide reductase A protects dopaminergic cells from Parkinson's disease-related insults. Free Radic. Biol. Med. 45, 242–255.
Low, P.A., et al., 2014. Efficacy and safety of rifampicin for multiple system atrophy: a randomised, double-blind, placebo-controlled trial. Lancet Neurol. 13, 268–275.
Maltsev, A.S., et al., 2013. Site-specific interaction between alpha-synuclein and membranes probed by NMR-observed methionine oxidation rates. J. Am. Chem. Soc. 135, 2943–2946.
Marley, J., et al., 2001. A method for efficient isotopic labeling of recombinant proteins. J. Biomol. NMR 20, 71–75.
Masuda, M., et al., 2006. Small molecule inhibitors of alpha-synuclein filament assembly. Biochemistry 45, 6085–6094.
Mazumder, P., et al., 2013. Insight into alpha-synuclein plasticity and misfolding from differential micelle binding. J. Phys. Chem. B 117, 11448–11459.
Nakamura, K., et al., 2011. Direct membrane association drives mitochondrial fission by the Parkinson disease-associated protein α-synuclein. J. Biol. Chem. 286, 20710–20726.
Nasstrom, T., et al., 2011. The lipid peroxidation products 4-oxo-2-nonenal and 4-hydroxy-2-nonenal promote the formation of alpha-synuclein oligomers with distinct biochemical, morphological, and functional properties. Free Radic. Biol. Med. 50, 428–437.
Necula, M., et al., 2003. Rapid anionic micelle-mediated alpha-synuclein fibrillization in vitro. J. Biol. Chem. 278, 46674–46680.
Ono, K., Yamada, M., 2006. Antioxidant compounds have potent anti-fibrillogenic and fibril-destabilizing effects for alpha-synuclein fibrils in vitro. J. Neurochem. 97, 105–115.
Ouberai, M.M., et al., 2013. alpha-Synuclein senses lipid packing defects and induces lateral expansion of lipids leading to membrane remodeling. J. Biol. Chem. 288, 20883–20895.
Pandey, A.P., et al., 2009. Clustering of alpha-synuclein on supported lipid bilayers: role of anionic lipid, protein, and divalent ion concentration. Biophys. J. 96, 540–551.
Parihar, M.S., et al., 2009. Alpha-synuclein overexpression and aggregation exacerbates impairment of mitochondrial functions by augmenting oxidative stress in human neuroblastoma cells. Int. J. Biochem. Cell Biol. 41, 2015–2024.
Pasanen, P., et al., 2014. A novel alpha-synuclein mutation A53E associated with atypical multiple system atrophy and Parkinson's disease-type pathology. Neurobiol. Aging 35 (2180), e1–e5.
Perrin, R.J., et al., 2000. Interaction of human α-synuclein and Parkinson's disease variants with phospholipids. Structural analysis using site-directed mutagenesis. J. Biol. Chem. 275, 34393–34398.
Perrin, R.J., et al., 2001. Exposure to long chain polyunsaturated fatty acids triggers rapid multimerization of synucleins. J. Biol. Chem. 276, 41958–41962.
Pfefferkorn, C.M., et al., 2012. Depth of alpha-synuclein in a bilayer determined by fluorescence, neutron reflectometry, and computation. Biophys. J. 102, 613–621.
Polymeropoulos, M.H., et al., 1997. Mutation in the α-synuclein gene identified in families with Parkinson's disease. Science 276, 2045–2047.
Proukakis, C., et al., 2013. A novel alpha-synuclein missense mutation in Parkinson disease. Neurology 80, 1062–1064.
Qin, Z., et al., 2007. Effect of 4-hydroxy-2-nonenal modification on alpha-synuclein aggregation. J. Biol. Chem. 282, 5862–5870.
Reynolds, N.P., et al., 2011. Mechanism of membrane interaction and disruption by alpha-synuclein. J. Am. Chem. Soc. 133, 19366–19375.
Rochet, J.C., et al., 2012. Molecular insights into Parkinson's disease. Prog. Mol. Biol. Transl. Sci. 107, 125–188.
Rutherford, N.J., et al., 2014. Divergent effects of the H50Q and G51D SNCA mutations on the aggregation of alpha-synuclein. J. Neurochem. 131, 859–867.
Scholtz, J.M., et al., 1991. Parameters of helix-coil transition theory for alanine-based peptides of varying chain lengths in water. Biopolymers 31, 1463–1470.
Sharon, R., et al., 2003. The formation of highly soluble oligomers of α-synuclein is regulated by fatty acids and enhanced in Parkinson's disease. Neuron 37, 583–595.
Shulman, J.M., et al., 2011. Parkinson's disease: genetics and pathogenesis. Annu. Rev. Pathol. 6, 193–222.
Shvadchak, V.V., et al., 2011a. Specificity and kinetics of alpha-synuclein binding to model membranes determined with fluorescent excited state intramolecular proton transfer (ESIPT) probe. J. Biol. Chem. 286, 13023–13032.
Shvadchak, V.V., et al., 2011b. The mode of alpha-synuclein binding to membranes depends on lipid composition and lipid to protein ratio. FEBS Lett. 585, 3513–3519.
Singleton, A.B., et al., 2003. alpha-Synuclein locus triplication causes Parkinson's disease. Science 302, 841.
Soper, J.H., et al., 2011. Aggregation of alpha-synuclein in *S. cerevisiae* is associated with defects in endosomal trafficking and phospholipid biosynthesis. J. Mol. Neurosci. 43, 391–405.
Spillantini, M.G., et al., 1997. α-Synuclein in Lewy bodies. Nature 388, 839–840.
Strathearn, K.E., et al., 2014. Neuroprotective effects of anthocyanin- and proanthocyanidin-rich extracts in cellular models of Parkinson's disease. Brain Res. 1555, 60–77.
Takamori, S., et al., 2006. Molecular anatomy of a trafficking organelle. Cell 127, 831–846.
Trexler, A., Rhoades, E., 2009. Alpha-synuclein binds large unilamellar vesicles as an extended helix. Biochemistry 48, 2304–2306.
Ulmer, T.S., et al., 2005. Structure and dynamics of micelle-bound human alpha-synuclein. J. Biol. Chem. 280, 9595–9603.
Vamvaca, K., et al., 2009. The first N-terminal amino acids of alpha-synuclein are essential for alpha-helical structure formation in vitro and membrane binding in yeast. J. Mol. Biol. 389, 413–424.
Venda, L.L., et al., 2010. alpha-Synuclein and dopamine at the crossroads of Parkinson's disease. Trends Neurosci. 33, 559–568.
Volles, M.J., Lansbury Jr., P.T., 2007. Relationships between the sequence of alpha-synuclein and its membrane affinity, fibrillization propensity, and yeast toxicity. J. Mol. Biol. 366, 1510–1522.
Wakabayashi, K., et al., 1998. α-Synuclein immunoreactivity in glial cytoplasmic inclusions in multiple system atrophy. Neurosci. Lett. 249, 180–182.
Weinreb, P.H., et al., 1996. NACP, a protein implicated in Alzheimer's disease and learning, is natively unfolded. Biochemistry 35, 13709–13715.
Winner, B., et al., 2011. In vivo demonstration that alpha-synuclein oligomers are toxic. Proc. Natl. Acad. Sci. U. S. A. 108, 4194–4199.
Zakharov, S.D., et al., 2007. Helical alpha-synuclein forms highly conductive ion channels. Biochemistry 46, 14369–14379.
Zarranz, J.J., et al., 2004. The new mutation, E46K, of alpha-synuclein causes Parkinson and Lewy body dementia. Ann. Neurol. 55, 164–173.
Zhang, H., et al., 2013. In vitro study of alpha-synuclein protofibrils by cryo-EM suggests a Cu(2+)-dependent aggregation pathway. Biophys. J. 104, 2706–2713.